Relative light units were normalized to the protein amounts determined with BCA Protein Assay Reagent (Pierce, Rockford, IL).

Microarray analysis. Primary cultures of cardiomyocytes, grown in serum-free medium OPTI-MEM for 24 h, were treated with vehicle (ethanol) or various ligands for 3 h with or without pretreatment of 10 μM RU-486. Total RNA was isolated using TRIZOL-Reagent (Invitrogen) according to the manufacturer's protocol and further purified using the RNeasy Mini Kit (Qiagen, Valencia, CA). We used pooled RNA samples from three independent experiments, and DNA microarray analysis were performed two times as follows: first experiment (vehicle, COR, ALD, or CVZ treatment) and second experiment (vehicle, COR, ALD, CVZ, RU-486, COR + RU-486, ALD + RU-486, or CVZ + RU-486 treatment). Using pooled RNA samples, preparation of the labeled cRNA and microarray hybridization were performed by Bio Matrix Research (Nagareyama, Japan) as follows. Isolated total RNA were amplified and labeled as described in the GeneChip Expression Analysis Technical Manual (Affymetrix, Santa Clara, CA). First, total RNA (1 μg) was converted into double-stranded cDNA using the One-Cycle cDNA Synthesis Kit (Affymetrix). Double-stranded cDNA was purified by using a GeneChip Sample Cleanup Module (Affymetrix). In vitro transcription reactions were performed using a GeneChip IVT Labeling Kit, which includes T7 RNA polymerase and Biotin-labeled ribonucleotides. Biotin-labeled cRNA was purified using a GeneChip Sample Cleanup Module. The concentration of cRNA was calculated from light absorbance at 260 nm using an ultraviolet spectrophotometer. Next, cRNA (15 μg) was fragmented at 94°C in the presence of a fragmentation buffer (Affymetrix). cRNA (15 μg) was hybridized to the Affymetrix GeneChip Rat Genome 230 2.0 Array (Affymetrix), on which 31,099 probe sets and 12,379 gene sets are represented. The array was incubated for 16 h at 45°C and then automatically washed and stained with the GeneChip Hybridization, Wash and Stain Kit (Affymetrix). The Probe Array was scanned using a GeneChip Scanner 3000 7G. The raw data were normalized and analyzed using GeneChip Affymetrix GCOS 1.2 software and GeneSpring 7.3.1 (Agilent Technologies, Palo Alto, CA). In per-chip normalization, a raw intensity value was divided by the median value of the chip measurements, and then, each gene was normalized to the respective control to enable relative changes in gene expression levels between samples. The signal values and the present (P flag), absent (A flag), or marginal (M flag) calls were computed for all probe, sets and only probe sets with the present call were used in the further analysis. Only the significantly expressed genes in both experiments were considered to be valid, and Ingenuity Pathway Analysis (http://www.Ingenuity.com; Ingenuity Systems, Redwood City, CA) was used to map those probes to genes with annotation, to perform pathway analysis, and to create gene networks. Functional classifications according to Gene Ontology (GO) terms were performed by using ExPlain (BIOBASE, Wolfenbüttel, Germany, www.biobase.de). The data discussed in this publication have been deposited in the National Center for Biotechnology Information's Gene Expression Omnibus [GEO (11)] and are accessible through GEO Series accession no. GSE12752 (http://www.ncbi.nlm.nih.gov/geo/query/acc.cgi?acc=GSE12752).

Real-time quantitative RT-PCR. Total RNA from primary cultures of cardiomyocytes was reverse-transcribed with oligo(dT) primers using the SuperScript III First-Strand Synthesis System for RT-PCR (Invitrogen). Real-time quantitative RT-PCR (qRT-PCR) was performed with the LightCycler TaqMan Master, Universal ProbeLibrary Set, Rat, and LightCycler ST300 systems (Roche, Basel, Switzerland) according to the manufacturer's instructions. Relative expression levels were calculated on the basis of standard curves generated for each gene, and mRNA for *glyceraldehyde-3-phosphate dehydrogense* (*Gapdh*) was used as an internal control. The primer sequences used in this study are as follows: *Gapdh*: 5′-agccacatcgctcagaca-3′ and 5′-gcccaatacgaccaaatcc-3′; *Klf15*: 5′-ctgcagcaagatgtacaccaa-3′ and 5′-tcatctgagcgtgaaaacctc-3′; *Bcat2*: 5′-gtcggtgactgcaagttgg-3′ and 5′-cctttcttctgggcttcttg-3′; *Slc2a4* (*glucose transporter 4, GLUT4*): 5′-tgcagtgcctgagtcttcttt-3′ and 5′-ccagtcactcgctgctga-3′; *Foxo1a*: 5′-tcaggctaggagttagtgagca-3′ and 5′-ggggtgaagggcatcttt-3′; *Fbxo32* (*atrogin-1*): 5′-cactctacactggcaacagca-3′ and 5′-ggtgatcgtgagacctttgaa-3′; *Gdf8* (*myostatin*): 5′-tgggcatgatcttgctgtaa-3′ and 5′-tgttactttgacttctaaaaagggatt-3′; *Sgk1*: 5′-ctcctatgcatgcaaacacc-3′ and 5′-tttgttgagagggacttggag-3′; *Nppb* (*brain natriuretic peptide, BNP*): 5′-gtcagtcgcttgggctgt-3′ and 5′-cagagctggggaaagaagag-3′; *Ptgs2* (*COX-2*): 5′-accaacgctgccacaact-3′ and 5′-gcccaatacgaccaaatcc-3′; and *Pla2g4a* (*cytoplasmic phospholipase A2, PLA2*): 5′-tctcatttaactctgggaactgc-3′ and 5′-cagctgcaggaattctcacac-3′.

Measurement of amino acid concentration. Measurement of amino acid concentration of cultured neonatal rat cardiomyocytes was performed as described previously (19) with minor modification. In brief, after medium replacement to the serum-free medium OPTI-MEM, cultured neonatal rat cardiomyocytes were infected or transfected with KLF15-expressing adenoviruses or siRNA oligonucleotides, respectively, and cultured for 24 h. Next, the medium was replaced to fresh OPTI-MEM, and the cells were further cultured with or without CVZ for 24 h. The cells were washed three times with PBS and lysed in 1 ml of ice-cold methanol for 5 min, except for the dish with the same protocols for counting the number of cells. Cellular lysates and recovery efficiency control Phe-d5 were collected in 15-ml tubes, 1 ml of chloroform was added to the lysates, and the mixtures were briefly voltexed. The mixtures were centrifuged at 1,000 *g*, 4°C for 5 min, and the supernatants were transferred to new 15-ml tubes. This chloroform precipitation method was again repeated, and the supernatants were concentrated and dried with a AES2010 SpeedVac system (Savant Instruments, Holbrook, NY) and redisolved in 200 μl of MilliQ ultra pure water (Millipore). Quantification of collected amino acid was performed with high-performance liquid chromatography-tandem mass spectrometry assay using Agilent 1100 HPLC (Agilent) interfaced to an Applied Biosystems/Sciex API 4000 triple quadrupole mass spectrometer (Applied Biosystems, Foster City, CA). Data collection and processing were performed with Sciex Analyst version 1.4.2 software (Applied Biosystems).

Statistical analysis. Except for DNA microarray analysis, we performed all experiments in triplicate, and the results are expressed as means ± SE of three independent experiments as indicated. The statistical significance of differences between groups was calculated either by one- or two-way ANOVA, and the difference was considered significant at $P < 0.05$.

RESULTS AND DISCUSSION

GR in rat cardiomyocytes and its ligand specificity. At first, to verify the feasibility to use isolated rat cardiomyocytes for identification of GR target genes, the presence of GR was confirmed in Western blot analyses. As shown in Fig. 1*A*, ligand-dependent nuclear localization of endogenous GR was clearly demonstrated in the presence of either endogenous or synthetic corticosteroids, COR and ALD, or CVZ, respectively, at the concentration of 100 nM for 1 h. Moreover, ligand-activated GR was shown to be able to induce expression of GRE-driven luciferase reporter gene (Fig. 1*B*). ALD, as previously reported (2, 38), appeared to be a weaker agonist compared with the other two glucocorticoids, since proportions of nuclear-translocated GR (Fig. 1*A*) and transactivation potential (Fig. 1*B*) were relatively smaller. We previously characterized CVZ as a GR-specific ligand without MR activation capacity (see introduction). To test whether this is also the case in rat GR and MR, we transfected the expression plasmids for rat GR or MR together with GRE-luciferase reporter gene in COS-7 cells. After treatment with 100 nM of COR or ALD, both rat GR and MR translocated in the nucleus. However,

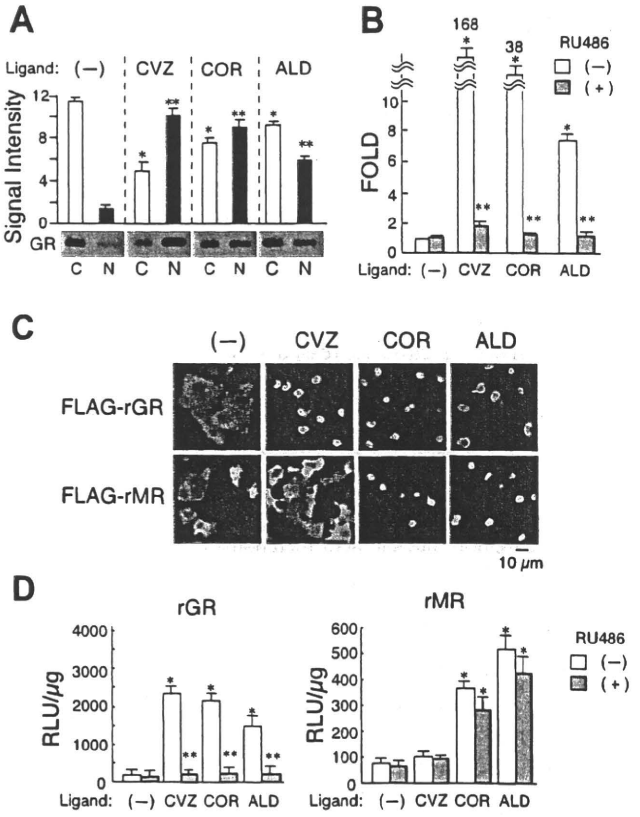

Fig. 1. Characterization of endogenous glucocorticoid receptor (GR) in rat cardiomyocytes and effects of synthetic and endogenous corticosteroids. *A*: subcellular localization of GR in neonatal rat cardiomyocytes. After treatment of the cardiomyocytes with or without 100 nM of each corticosteroid for 1 h as indicated, cytosolic extracts (C) and nuclear extracts (N) were prepared, Western immunoblotting for GR were performed, and signal intensity of the band for GR relative to that for α-actinin of each extract was quantified as described in MATERIALS AND METHODS. Means ± SE of 3 independent experiments and representative photographs are shown. $P < 0.05$ vs. cytosolic extract treated with vehicle (*) and vs. nuclear extracts treated with vehicle (**). CVZ, cortivazol; COR, corticosterone; ALD, aldosterone. *B*: effect of corticosteroids on glucocorticoid response element (GRE)-dependent reporter gene expression in neonatal rat cardiomyocytes. The cardiomyocytes were transfected with 2 μg of reporter plasmids p2xGRE-LUC and treated with 100 nM of each ligand as indicated in the presence (filled bars) or absence (open bars) of 10 μM RU-486 for 24 h. Results are expressed as relative expression levels to the vehicle-treated samples and means ± SE of 3 independent experiments are shown. $P < 0.05$ vs. cells treated with vehicle (*) and vs. RU-486 (−; **). *C*: ligand specificity of rat GR and mineralocorticoid receptor (MR) nuclear translocation. COS-7 cells expressing either FLAG-tagged rat GR or MR were cultured with or without 100 nM of each ligand as indicated for 2 h, and immunofluorescent analysis was performed as described in MATERIALS AND METHODS. Experiments were repeated 3 times with almost identical results, and representative results are shown. *D*: ligand specificity of rat GR and MR reporter gene assay. COS-7 cells were cotransfected with 2 μg of reporter plasmids p2xGRE-LUC and 100 ng of either p3xFLAG-rGR or p3xFLAG-rMR and were cultured with 100 nM of each ligand as indicated in the presence (filled bars) or absence (open bars) of 10 μM RU-486 for 24 h. Results are expressed as relative light units (RLU)/μg of protein in the extract, and means ± SE of 3 independent experiments are shown. $P < 0.05$ vs. cells treated with vehicle (*) and vs. RU-486 (−; **).

CVZ failed to promote nuclear translocation of not GR but MR (Fig. 1*C*). This issue is further supported by the luciferase assay in which CVZ again failed to induce MR-dependent reporter gene activation (Fig. 1*D*). It was also shown that the GR antagonist RU-486 shut down GR-dependent GRE-luciferase reporter gene activation by either CVZ, COR, or ALD; however, RU-486 did not repress ALD or COR-inducible MR-dependent reporter gene activation (Fig. 1, *B* and *D*). We, therefore, concluded that CVZ and RU-486 are useful to differentiate GR-dependent gene expression profile from that of MR as GR-specific agonist and antagonist, respectively.

Global analysis of gene expression after treatment with corticosteroids in rat cardiomyocytes. To identify which set of gene expression is influenced by GR, we analyzed gene expression changes after exposure of cells to COR, ALD, and CVZ in the absence or presence of RU-486. Because our preliminary experiments using several cell lines showed that expression of many GR target genes was induced by COR at the concentration of 100 nM in 3 h and previous reports indicated that a concentration of 100 nM of COR was considered to be equivalent to maximal and supraphysiological level in cultured cells (13, 22), we in the present study set the concentration of these ligands and the time periods of exposure as 100 nM and 3 h, respectively. We also expected that this relatively short exposure would avoid secondary effects of the products of GR-regulated genes. The results of our microarray analyses were summarized in Fig. 2 and Table 1 [the detailed results were uploaded in Supplemental Table 1 (Supplemental data for this article can be found on the *American Journal of Physiology-Endocrinology and Metabolism* website)]. Among 12,379 genes, 7,351, 7,478, 7,507, 7,803, 7,863, and 7,845 genes were considered to be relevant for further analysis for CVZ-, COR-, ALD-, CVZ + RU-486-, COR + RU-486-, and ALD + RU-486-treated cells, respectively (see MATERIALS AND METHODS for details). Four hundred genes were significantly induced, and 57 genes were repressed after treatment with either CVZ, COR, or ALD (Table 1). For classification, a Venn diagram was applied, and it was revealed that treatment with CVZ, COR, and ALD induced 351 (*categories 1*, *4*, *6*, and *7*), 192 (categories 2, 4, 5 and 7), and 87 (*categories 3*, *5*, *6*, and *7*) genes, respectively, with significant overlap between each (Fig. 2*A*). RU-486 sensitivity of the genes in *categories 1*, *4*, and *7* was 91.1% (for CVZ), 95.1% (for CVZ) and 79.6% (for COR), and 94.6% (for CVZ) and 75% (for COR), respectively (Table 1). We, therefore, may indicate that expression of the majority of those genes induced by CVZ or COR in *categories 1*, *4*, and *7* was considered to be mediated through GR. Indeed, the gene set that was induced by CVZ and COR (*categories 4* and *7*) contained many classical glucocorticoid-regulated genes, e.g., PDK4, SGK, and FKBP5, and the fold inducibility appeared to be greater in CVZ than in COR or ALD (Supplemental Table 1). When CVZ and COR were compared, 159 genes were induced by both CVZ and COR, corresponding to *categories 4* and *7*, but 192 genes (54.7% of CVZ-induced genes, corresponding to *categories 1* and *6*) were induced not COR but by CVZ, and 33 (17.2% of COR-induced genes, corresponding to *categories 2* and *5*) were induced by COR but not by CVZ. Considering that CVZ has stronger agonistic activity compared with COR or ALD, it was unexpected that these 33 genes (*category 2* and *5*) were not induced by CVZ. RU-486 sensitivity of those 33 genes belonging to *categories 2* and *5* was slightly lower (60.6% for COR) than that of 192 genes of *categories 1* and *6* (89.5% for CVZ). Concerning the genes in *categories 2* and *5*, fold inducibility by COR was marginal, and RU-486 sensitivity was equivocal (Supplemental

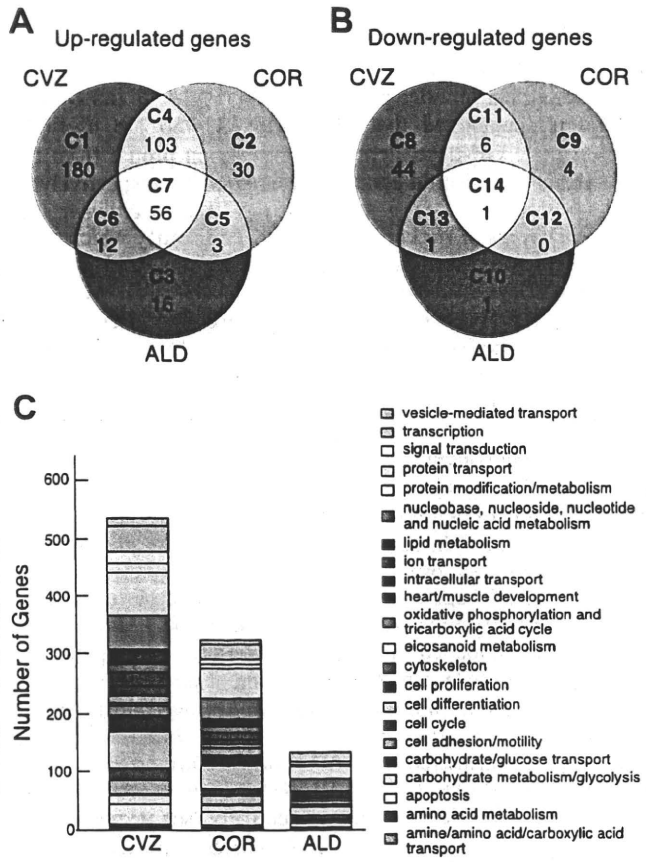

Fig. 2. Venn diagrams of corticosteroid-induced (*A*) or -repressed (*B*) genes and Gene Ontology analysis (*C*). *A* and *B*: venn diagrams. After isolation of total RNA from neonatal rat cardiomyocytes treated with either CVZ, COR, or ALD, with or without RU-486, DNA microarray analysis was performed, and data mining was done as described in MATERIALS AND METHODS. Venn diagrams illustrate the overlaps in CVZ, COR, and ALD target genes. The category numbers (C1–C14) and the number of upregulated (>1.5-fold vs. vehicle; *A*) and downregulated (<0.5-fold vs. vehicle; *B*) genes are depicted (See Table 1 and Supplemental Table 1 for details). *C*: Gene Ontology. The gene set induced by each corticosteroid was functionally classified according to Gene Ontology terms by using ExPlain software as described in MATERIALS AND METHODS, and results are shown.

Table 1); it appears that the mode of their gene expression might be distinct from that of canonical GR target genes. Interestingly, RU-486 sensitivity of the genes in *category 7* appeared to be lower in ALD-induced cases than in CVZ- or COR-induced cases (Supplemental Table 1), suggesting that RU-486 sensitivity of not all but some GR target genes may be influenced by ligand context.

Concerning ALD action, mRNA expression of 87 genes was induced by ALD (*categories 3*, *5*, *6*, and *7*). Among 384 genes that were induced by either CVZ or COR (*categories 1*, *2*, *4*, *5*, *6*, and *7*), only 71 genes (18.5% of 384 genes) were induced by ALD (81.6% of 87 ALD-induced genes). When the genes belonging to *category 7* were excluded, we could not find known glucocorticoid-regulated genes in the ALD-induced gene set. Moreover, fold inducibility of the majority of ALD-induced genes appeared to be marginal (Supplemental Table 1), and RU-486 sensitivity was relatively low (50, 66.7, 50, 41.1% for ALD, in *categories 3*, *5*, *6*, and *7*, respectively) (Table 1). We, thus, may consider that, at least as far as a number of induced genes and their fold inducibility, glucocorticoids appear to be a major determinant of GR-mediated gene expression in cardiomyocytes.

The total number of downregulated genes (n = 57) was smaller than that of upregulated genes (n = 400) in rat cardiomyocytes, and again CVZ appeared to be stronger than COR or ALD (Supplemental Table 1 and Fig. 2*B*). In clear contrast to transcriptional induction, RU-486 is known to have a similar transrepressive effect when compared with agonistic glucocorticoids, including CVZ and COR (17). The ligand-based approach, therefore, did not appear to be merited in further analysis of those repressed genes, and we focused on the induced genes in the following sections.

GO analysis of corticosteroid target genes. Results of GO analysis were represented as boxed charts in Fig. 2*C*. The pattern of the charts was similar between CVZ-induced genes and COR-induced ones; these ligands influenced such genes belonging to, for example, protein modification/metabolism, cell differentiation, nucleic acid metabolism, transcription, apoptosis, and lipid metabolism. However, the number of genes in each category was drastically different between CVZ-induced genes and COR-induced ones (Fig. 2*C*). We (52, 53) and others (49) previously indicated that CVZ may have distinct target gene sets when compared with natural glucocorticoids, since CVZ has a phenylpyrazol moiety at the A ring of steroid structure. Indeed, Miller et al. (32) also revealed that, while CVZ and DEX overlap in regulation of most genes, each steroid regulates expression of an exclusive set of transcripts in CEM-C7-14 cells (sensitive to apoptosis by both DEX and CVZ) and CEM-C1-15 cells (DEX-resistant but CVZ-sensitive). Moreover, they showed that 57 genes were regulated uniquely to a statistically significant extent by CVZ in both clones and many of the CVZ specific genes are key components of various signal transduction pathways and not all but some are related to apoptosis. The fact that the order of the number of induced genes was CVZ > COR > ALD in our study may support such an idea that CVZ may have a distinct target gene set.

These gene expression profiles suggested numerous roles of corticosteroids in various aspects of cardiac physiology and that glucocorticoids and mineralocorticoid, and GR and MR as well, appeared to have distinct sets of target genes in cardiomyocytes. For example, among others, corticosteroids induced mRNA expression of FKBP5 via GR, in the descending rank order of CVZ, COR, and ALD, with efficient suppression by RU-486 (Supplemental Table 1). It, therefore, may be concluded that FKBP5 gene expression is driven by the glucocorticoid-GR axis. Because FKBP5 is shown to be contained in GR chaperon complex with heat shosk protein-90, this result may indicate that the ultrashort feedback loop of GR operates in cardiomyocytes (4). Glucocorticoids have been known to induce myocardial hypertrophy in vivo, however, and the effects of glucocorticoids on the cell size of cardiomyocytes are still controversial in vitro (10, 14, 26, 51). Indeed, several reports have suggested that treatment of cardiomyocytes with COR alone has had a little effect for the cell growth and enlargement (24, 28). In our experimental settings, DNA microarray and qRT-PCR analysis revealed that, in cultured cardiomyocytes, CVZ and COR induced mRNA expression of several prohypertrophic genes such as SGK and BNP (Supple-

Table 1. *Classification of corticosteroid-induced and -repressed genes in DNA microarray analysis*

Category	Total	CVZ		COR		ALD	
		RU sensitive	RU insensitive	RU sensitive	RU insensitive	RU sensitive	RU insensitive
				No. of Upregulated Genes			
C1	180	164	16	0	0	0	0
C2	30	0	0	19	11	0	0
C3	16	0	0	0	0	8	8
C4	103	98	5	82	21	0	0
C5	3	0	0	1	2	2	1
C6	12	8	4	0	0	6	6
C7	56	53	3	42	14	23	33
Total	400	323	28	144	48	39	48
				No. of Downregulated Genes			
C8	44	38	6	0	0	0	0
C9	4	0	0	2	2	0	0
C10	1	0	0	0	0	0	1
C11	6	6	0	4	2	0	0
C12	0	0	0	0	0	0	0
C13	1	0	1	0	0	0	1
C14	1	0	1	0	1	0	1
Total	57	44	8	6	5	0	3

No. of genes grouped by the category classified in Venn diagrams as shown in Fig. 2 together with the presence or absence of antagonism by RU-486 (RU-sensitive or -insensitive, respectively) for upregulated (>1.5-fold) or downregulated (<0.5-fold) genes in DNA microarray analysis as described in MATERIALS AND METHODS. RU-486-sensitive, $([X + \text{RU-486}] - 1)/([X] - 1) < 0.5$; RU-insensitive, $([X + \text{RU-486}] - 1)/([X] - 1) > 0.5$ [X is either cortivazol (CVZ), corticosterone (COR), or aldosterone (ALD), and square brackets depict fold induction in Supplemental Table 1].

mental Table 1 and Fig. 3). In contrast, CVZ and COR also induced mRNA expression of atrophy-related genes, i.e., FOXO1a, atrogin-1, and myostatin (Supplemental Table 1 and Fig. 3), which are known as the regulators of muscle mass via the ubiquitin-proteasome pathway (30). CVZ or COR treatment of cultured cardiomyocytes for 72 h did not significantly affect their cell size (data not shown). Together, it is indicated that glucocorticoids have distinct sets of target genes in cardiomyocytes, and, among them, balance between prohypertrophic genes and proapoptotic genes might, at least in part, determine cell size. Such balance might be regulated not only by glucocorticoids but also by various extra- and/or intracellular factors, e.g., hypertension and metabolic status. Indeed, it has been reported that glucocorticoid-induced cardiac enlargement of the rat heart was transient, and extension of treatment duration with a high level of glucocorticoid brought about anabolic to catabolic state transformation with the loss of the cardiac growth (6, 25).

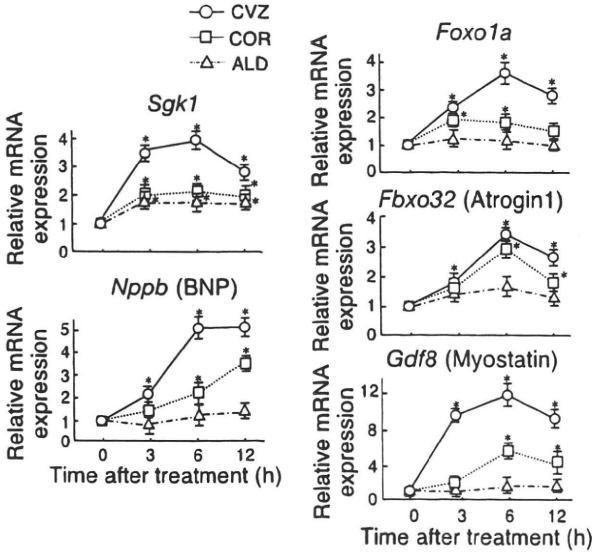

Fig. 3. Time course of mRNA expression of glucocorticoid-regulated genes in rat cardiomyocytes. Total RNA was isolated from neonatal rat cardiomyocytes after treatment with 100 nM CVZ (circles), COR (squares), or ALD (triangles) for the indicated time periods, and was analyzed in qRT-PCR as described in MATERIALS AND METHODS. mRNA expression levels were normalized to *glyceraldehyde-3-phosphate dehydrogenase* (*Gapdh*) and relative expression levels to the 0-h samples are presented. Means ± SE of 3 independent experiments are shown. BNP, brain natriuretic peptide. $^*P < 0.05$ vs. cells treated with each ligand at 0 h.

Of note, it was revealed that glucocorticoids induce mRNA expression of numerous transcription factors, including FOXO1a, C/EBPβ, PGC-1α, and a member of Kruppel-like transcription factors KLF9 and KLF15 (Supplemental Table 2). Their induction response was greater in CVZ and COR than in ALD and significantly repressed by RU-486, and their mRNA expression is also considered to be transcriptionally regulated by GR (Supplemental Table 2). Because not all but many of them are known to be involved in various metabolic processes (9), our results may indicate that glucocorticoid-GR modulates complex metabolic milieus via cascade of regulation of gene expression in the heart.

Glucocorticoid-mediated amino acid catabolism via the KLF15 pathway. In the present study, Ingenuity Pathway Analysis returned the highest score to the gene network involving KLF15 and correlating with cardiovascular system development and function, amino acid metabolism, and small molecular biochemistry (Supplemental Table 3). KLFs are a subclass of the zinc finger family of DNA-binding transcription factors, and recent studies have revealed the physiological importance of several members of the KLF family in the heart and vessels (3). Especially, KLF15 was recently reported to be an inhibitor of cardiac hypertrophy (12). KLF15 is also con-

sidered to be involved in amino acid catabolism to induce branched-chain aminotransferase 2 (BCAT2) gene expression, which is rate-limiting for amino acid breakdown in skeletal muscle and increases alanine production for liver gluconeogenesis (12).

We showed that glucocorticoids induce mRNA expression of KLF15 in cardiomyocytes. This issue was further supported by qRT-PCR analysis and siRNA experiments; after treatment with not ALD but CVZ or COR in cardiomyocytes, mRNA expression of KLF15 was rapidly increased (from 3 h after treatment with corticosteroids) in a time- and concentration-dependent manner (Fig. 4, *A* and *B*). Moreover, such induction response was cancelled by introduction of siRNA against GR (Fig. 4*C*), indicating that mRNA induction of KLF15 is mediated through GR. It is known that gene expression of BCAT2 and GLUT4 is transcriptionally controlled by KLF15 (12, 15). We showed that mRNA expression of BCAT2 and GLUT4 (Slc2a4) genes was increased after treatment with CVZ and COR with a lag time of ~3–6 h after apparent induction of KLF15 mRNA in cardiomyo-

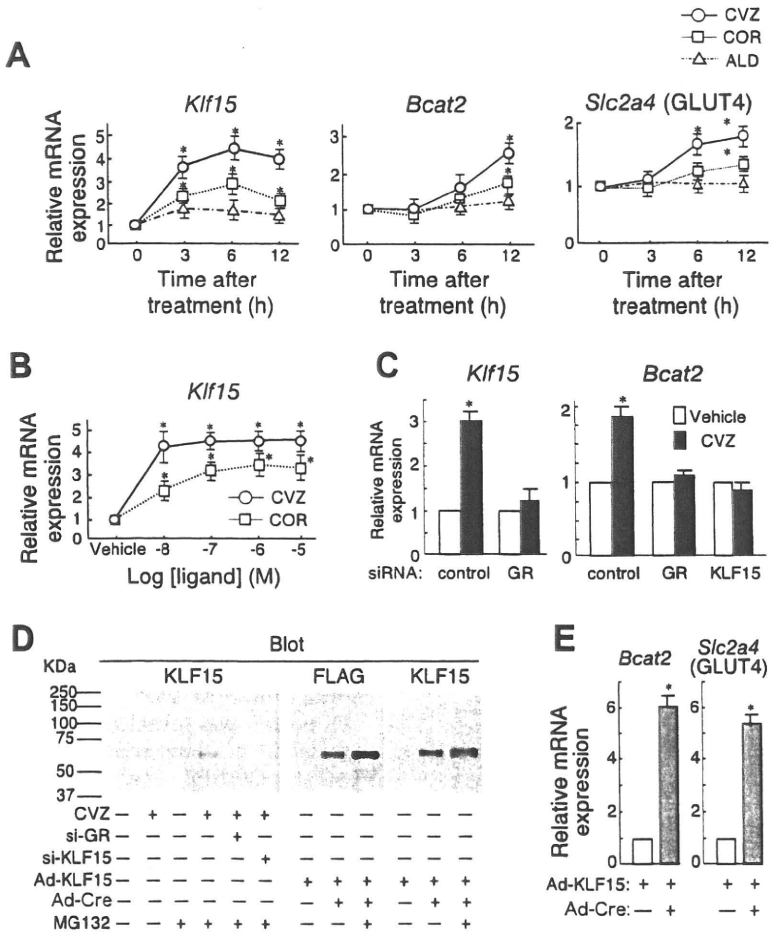

Fig. 4. KLF15 is a GR target gene involved in the amino acid catabolic pathway in rat cardiomyocytes. *A*: time course of mRNA expression of KLF15 and its target genes. Total RNA was isolated from neonatal rat cardiomyocytes after treatment with 100 nM of CVZ (circles), COR (squares), or ALD (triangles) for the indicated time periods and was analyzed in qRT-PCR as described in MATERIALS AND METHODS. mRNA expression levels were normalized to *Gapdh*, and relative expression levels to the 0-h samples are presented. Means ± SE of 3 independent experiments are shown. $*P < 0.05$ vs. cells treated with each ligand at 0 h. *B*: concentration-dependent regulation of KLF15 gene expression by glucocorticoids. Total RNA was isolated from neonatal rat cardiomyocytes after treatment with the indicated concentrations of CVZ (circles) or COR (squares) for 3 h. mRNA expression levels were normalized to *Gapdh*, and relative expression levels to the vehicle-treated samples are presented. Means ± SE of 3 independent experiments are shown. $*P < 0.05$ vs. cells treated with vehicle. *C*: effect of GR knockdown on glucocorticoid-dependent induction of mRNA expression of KLF15 and BCAT2. The cardiomyocytes were transfected with control small-interfering RNA (siRNA) or siRNA oligonucleotides for GR, KLF15 as indicated, and cultured for 24 h. Next, the cells were treated with vehicle or 100 nM CVZ for 12 h, and total RNA was analyzed with qRT-PCR. Results were normalized to *Gapdh*, and relative expression levels to vehicle-treated samples are presented. Means ± SE of 3 independent experiments are shown. $*P < 0.05$ vs. vehicle-treated cells. *D*: Western blot analysis for KLF15 protein. Control siRNA, siRNA against GR (si-GR), siRNA against KLF15 (si-KLF15), Cre-expressing adenoviruses [Ad-Cre, multiplicity of infection (MOI) = 5], and floxed FLAG-tagged KLF15-expressing adenoviruses (Ad-KLF15, MOI = 10) were introduced in cardiomyocytes and were cultured in the presence or absence of 5 μM MG-132 for 12 h as indicated. Next, whole cell extracts were prepared, and Western immunoblot was performed with anti-KLF15 antibodies (*left* and *right*) and anti-FLAG antibodies (*middle*). Experiments were repeated 3 times with almost identical results, and representative photographs are shown. *E*: induction of mRNA expression of BCAT2 and GLUT4 by KLF15. Ad-Cre and Ad-KLF15 were infected in rat cardiomyocytes as indicated, and the cells were cultured for 24 h. Total RNA was prepared and analyzed with qRT-PCR. Results were normalized to *Gapdh*, and results are expressed as relative expression levels to Ad-KLF15(−) cells. Means ± SE of 3 independent experiments are shown. $*P < 0.05$ vs. Ad-KLF15(−) cells.

cytes (Fig. 4*A*). In addition, the fact that siRNA for either GR or KLF15 shut down hormone-dependent induction of BCAT2 mRNA expression (Fig. 4*C*) strongly argues the critical importance of the glucocorticoid-GR-KLF15 pathway for BCAT2 gene expression.

Next, we further addressed the role of GR-dependent KLF15 induction in cardiomyocytes. In Western blot analysis, the KLF15 protein band was not detected after treatment of cardiomyocytes with CVZ alone. However, addition of the proteasome inhibitor MG-132 generated significant signal for KLF15 protein in the presence of CVZ, which was canceled in the copresence of siRNA against GR or KLF15. Infection of adenovirus carrying flag-tagged KLF15 in cardiomyocytes induced exogenous KLF15 protein expression, which was again increased by MG132 treatment (Fig. 4*D*). These results further confirmed the role of glucocorticoids for cardiac KLF15 expression and suggested that KLF15 may be a labile and rapid turnover protein. Using this adenoviral system, we revealed that overexpression of KLF15 in cardiomyocytes significantly increased mRNA expression of BCAT2 and GLUT4 (Fig. 4*E*).

Next, we examined the role of glucocorticoids and KLF15 on amino acid metabolism in rat cardiomyocytes. Adenovirus-mediated overexpression of KLF15 decreased the concentrations of Val, Leu, and Ile (Fig. 5*A*), indicating that KLF15, most possibly via BCAT2 induction, may degrade branched-chain amino acid (BCAA). As previously reported (41), treatment of cardiomyocytes with CVZ upregulated mRNA expression of glutamine synthase, which catalyses condensation of Glu and ammonia to form Gln (Supplemental Table 1, and also see Ref. 21) and increased Gln with a reciprocal decrease in Glu (Fig. 5*B*). However, this alteration in the concentrations of Glu to Gln was not affected by siRNA-mediated knockdown of KLF15 (Fig. 5*B*). In clear contrast, the concentrations of Val, Leu, and Ile were decreased after treatment with CVZ and affected by KLF15 knockdown (Fig. 5*B*). At this moment, the precise role of BCAA in cardiac physiology remains unknown. In peripheral tissues, BCAA is shown to play an important role in multiple metabolic processes, including regulation of insulin sensitivity, protein synthesis, and energy production and expenditure (18, 23, 43). Further study, therefore, might clarify an as yet unidentified physiological role of glucocorticoids via alteration in amino acid composition in the heart.

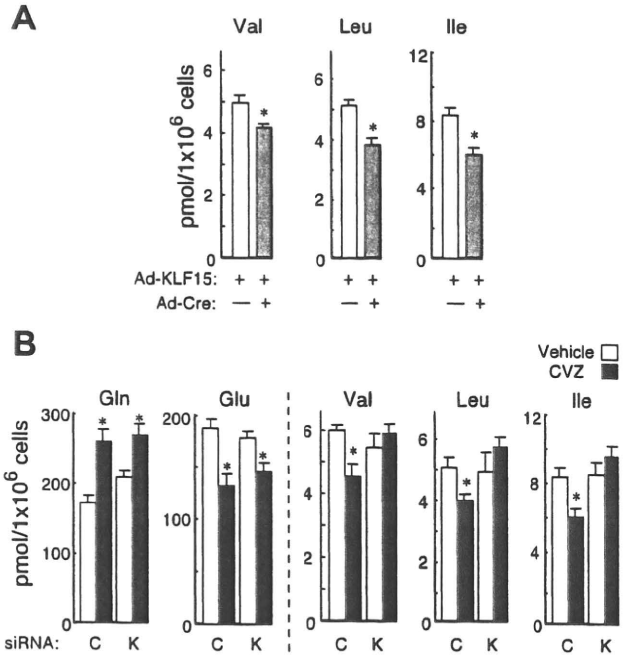

Fig. 5. Effects of glucocorticoid on intracellular concentration of amino acids. *A*: overexpression of KLF15 reduces the intracellular concentration of branched-chain amino acid (BCAA) in cardiomyocytes. Ad-Cre and Ad-KLF15 were infected in cultured rat cardiomyocytes, and the cells were cultured with fresh medium for 24 h. Measurement of amino acid concentration was performed as described in MATERIALS AND METHODS, and results are presented with means ± SE of 3 independent experiments. $*P < 0.05$ vs. Ad-KLF15(−) cells. *B*: glucocorticoid differentially modulates amino acid concentration in rat cardiomyocytes. The cardiomyocytes were transfected with siRNA oligonucleotides for KLF15 (K) or control (C) as indicated and cultured for 24 h. Next, the cells were treated with vehicle or 100 nM CVZ for 24 h. Results are presented with means ± SE of 3 independent experiments. $*P < 0.05$ vs. vehicle-treated cells.

Glucocorticoids enhance prostaglandin biosynthesis via GR. GO analysis also revealed the role of glucocorticoids in lipid metabolism in rat cardiomyocytes (Supplemental Table 2). Notably, it was striking that glucocorticoid-GR signaling promotes gene expression of the enzymes involved in the prostaglandin biosynthesis, including PLA2 and COX-2 in cardiomyocytes (Supplemental Tables 1 and 2), since this issue appears to be contradictory to the current knowledge that glucocorticoids elicit their anti-inflammatory properties via suppression of inflammatory induction of PLA2 and COXs and subsequent synthesis of proinflammatory prostaglandins (37). However, we confirmed our microarray data in qRT-PCR. As shown in Fig. 6, *A* and *B*, CVZ and COR significantly induced mRNA expression of these genes in a dose-dependent fashion, and these gene expressions were efficiently canceled by the GR antagonist RU-486. Moreover, introduction of siRNA against GR diminished the glucocorticoid-mediated upregulation of mRNA expression of PLA2 and COX-2 (Fig. 6*C*). We also confirmed this issue at protein levels in Western blot analysis as well. COX-2 protein expression was enhanced by 10.5- and 2.8-fold after treatment with CVZ and COR, respectively. On the other hand, other steroid hormones, including ALD, estradiol, and progesterone, did not significantly induce COX-2 protein expression (Fig. 6*D*). This glucocorticoid-mediated upregulation of COX-2 protein expression was almost comparable to that after treatment with IL-1β and lipopolysaccharide and was not observed in cardiac fibroblasts (Fig. 6*D* and data not shown). Glucocorticoid also induced mRNA expression of COX-1 and prostaglandin D_2 synthase by a lesser degree compared with that of COX-2 and PLA2 (Supplemental Table 1 and data not shown).

During the preparation of this manuscript, it was reported that COX-2 are induced by glucocorticoids in cultured rat cardiomyocytes (46). Our present work strongly indicates that glucocorticoid triggers the production of a certain class of prostaglandins/eicosanoids via induction of mRNA expression of these enzymes. Recently, it was shown that both COX-1 and COX-2 are expressed in the myocardium and that selective COX inhibitor caused an incomplete inhibition of prostaglandin E_2 (PGE_2) production from heart muscle (47), indicating that both COX isoforms are enzymatically active and contribute to PGE_2 generation in the myocardium. Using cultures of

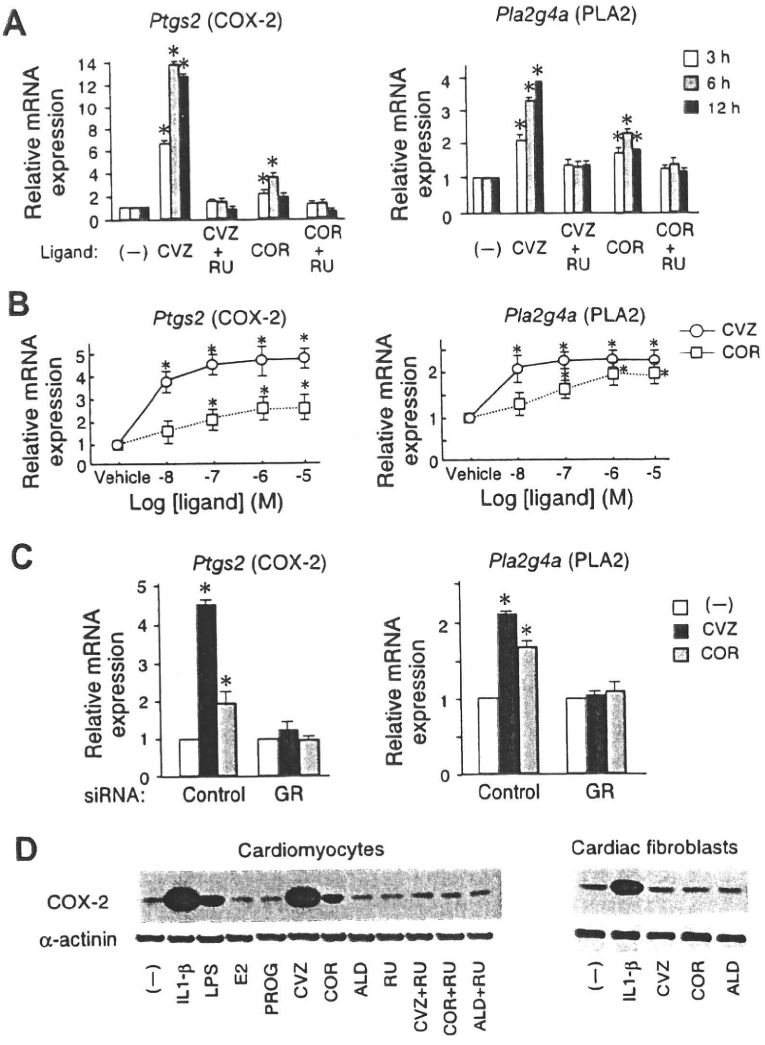

Fig. 6. Glucocorticoids regulate prostaglandin metabolism in the cardiomyocytes. *A*: time course of mRNA expression of *Ptgs2* (cyclooxigenase-2; COX-2) and *Pla2g4a* (cytoplasmic phospholipase A2; PLA2) in neonatal rat cardiomyocytes. The cells were cultured in the presence of each ligand for the indicated time periods, and mRNA expression of COX-2 and PLA2 was determined with qRT-PCR as described in MATERIALS AND METHODS. mRNA expression levels were normalized to *Gapdh* mRNA, and relative expression levels to the vehicle-treated samples at each time point are presented as fold (means ± SE of 3 independent experiments are shown). RU, RU-486. $*P < 0.05$ vs. cells treated with vehicle. *B*: concentration-dependent regulation of *Ptgs2* and *Pla2g4a* gene expression by glucocorticoids. Total RNA was isolated from neonatal rat cardiomyocytes after treatment with the indicated concentrations of CVZ (circles) or COR (squares) for 3 h and analyzed in qRT-PCR as described in MATERIALS AND METHODS. $*P < 0.05$ vs. cells treated with vehicle. *C*: effect of GR knockdown on glucocorticoid-dependent induction of mRNA expression of COX-2 and PLA2. Neonatal rat cardiomyocytes were transfected with siRNA oligonucleotide for GR or control siRNA as indicated and cultured for 24 h. Next, the cells were treated with vehicle or 100 nM CVZ and COR for 12 h. Total RNA was prepared and analyzed with qRT-PCR. $*P < 0.05$ vs. vehicle-treated cells. *D*: effects of glucocorticoids on COX-2 protein expression in neonatal rat cardiomyocytes. Rat cardiomyocytes (*left*) or cardiac fibroblasts (*right*) were treated with vehicle or 10 ng/ml interleukin (IL)-1β, 100 ng/ml lipopolysaccharide (LPS), 100 nM each of estradiol (E2), progesterone (PROG), CVZ, COR, ALD, or 10 μM RU-486 (RU). Whole cell extracts were prepared, and 10 μg of protein were separated in SDS-PAGE. Protein expression of COX-2 and α-actinin was analyzed in Western blot as described in MATERIALS AND METHODS. Experiments were repeated 3 times with almost identical results, and representative results are shown.

rat neonatal ventricular myocytes, Mendez and Lapointe (31) demonstrated an induction of COX-2 in vitro. Liu and coworkers (29) found a constitutive expression of both COX isoforms in rat hearts, which was enhanced by lipopolysaccharide infused in vivo. The biological function of COX-2 in the cardiomyocytes might be of major clinical concern, since the pharmacological role of COX-2 inhibitor still remains to be clarified (7). Further study is now ongoing to identify which eicosanoid products are mainly generated in cardiomyocytes under exposure to excess glucocorticoids and to clarify the role of such products in cardiac physiology.

In conclusion, our ligand-based approach involving CVZ and RU-486 as well as COR and ALD appears to be powerful to comprehensively identify target genes of the glucocorticoid-GR system. We think that such an approach could be applicable to an in vivo model as well as cultured cells. Because GR-MR redundancy is hazardous for identification of physiological function of corticosteroids in nonepithelial tissues that express both receptors but not 11β-HSD2, our approach may be deserved for such purposes.

Recent basic and clinical studies have highlighted the role of corticosteroid signaling in cardiac physiology and pathophysiology. Our ligand-based microarray analyses have clearly demonstrated that glucocorticoid-GR signaling may play various roles via alteration in the gene expression program and control complexed metabolic milieus in cardiomyocytes. Because ALD did not significantly contribute to expression of a majority of those genes that were induced via GR, we may strengthen that not MR but rather GR signaling should have important roles for maintenance of cardiomyocyte function, at least in the neonatal stage. Moreover, it is of particular interest that glucocorticoids are shown to be involved in amino acid catabolism and prostaglandin biosynthesis in the heart. In any case, further studies, therefore, should be performed to clarify how these corticosteroid-receptor systems coordinatedly regulate the gene expression program in concert with endocrine systems and contribute to maintenance of cardiac function.

ACKNOWLEDGMENTS

We thank Takako Maruyama for excellent technical assistance, members of the Morimoto Laboratory for help and discussion, and Drs. S. Nishitani, N. Ono, and K. Takehana (Pharmaceutical Research Laboratories, Ajinomoto) for excellent technical assistance in amino acid analysis.

GRANTS

This work was partly supported by a grant for Research on Intractable Diseases from the Japanese Ministry of Health, Labour and Welfare, KAKENHI (17GS0419, 20790657), and Nakatomi Foundation.

REFERENCES

1. **Almon RR, DuBois DC, Yao Z, Hoffman EP, Ghimbovschi S, Jusko WJ.** Microarray analysis of the temporal response of skeletal muscle to methylprednisolone: comparative analysis of two dosing regimens. *Physiol Genomics* 30: 282–299, 2007.
2. **Arriza JL, Weinberger C, Cerelli G, Glaser TM, Handelin BL, Housman DE, Evans RM.** Cloning of human mineralocorticoid receptor complementary DNA: structural and functional kinship with the glucocorticoid receptor. *Science* 237: 268–275, 1987.
3. **Atkins GB, Jain MK.** Role of Kruppel-like transcription factors in endothelial biology. *Circ Res* 100: 1686–1695, 2007.
4. **Binder EB, Bradley RG, Liu W, Epstein MP, Deveau TC, Mercer KB, Tang Y, Gillespie CF, Heim CM, Nemeroff CB, Schwartz AC, Cubells JF, Ressler KJ.** Association of FKBP5 polymorphisms and childhood abuse with risk of posttraumatic stress disorder symptoms in adults. *J Am Med Assoc* 299: 1291–1305, 2008.
5. **Brotman DJ, Girod JP, Garcia MJ, Patel JV, Gupta M, Posch A, Saunders S, Lip GY, Worley S, Reddy S.** Effects of short-term glucocorticoids on cardiovascular biomarkers. *J Clin Endocrinol Metab* 90: 3202–3208, 2005.
6. **Czerwinski SM, Kurowski TT, McKee EE, Zak R, Hickson RC.** Myosin heavy chain turnover during cardiac mass changes by glucocorticoids. *J Appl Physiol* 70: 300–305, 1991.
7. **Davies NM, Jamali F.** COX-2 selective inhibitors cardiac toxicity: getting to the heart of the matter. *J Pharm Pharm Sci* 7: 332–336, 2004.
8. **Davis JM 3rd, Maradit Kremers H, Crowson CS, Nicola PJ, Ballman KV, Therneau TM, Roger VL, Gabriel SE.** Glucocorticoids and cardiovascular events in rheumatoid arthritis: a population-based cohort study. *Arthritis Rheum* 56: 820–830, 2007.
9. **Desvergne B, Michalik L, Wahli W.** Transcriptional regulation of metabolism. *Physiol Rev* 86: 465–514, 2006.
10. **de Vries WB, van der Leij FR, Bakker JM, Kamphuis PJ, van Oosterhout MF, Schipper ME, Smid GB, Bartelds B, van Bel F.** Alterations in adult rat heart after neonatal dexamethasone therapy. *Pediatr Res* 52: 900–906, 2002.
11. **Edgar R, Domrachev M, Lash AE.** Gene Expression Omnibus: NCBI gene expression and hybridization array data repository. *Nucleic Acids Res* 30: 207–210, 2002.
12. **Fisch S, Gray S, Heymans S, Haldar SM, Wang B, Pfister O, Cui L, Kumar A, Lin Z, Sen-Banerjee S, Das H, Petersen CA, Mende U, Burleigh BA, Zhu Y, Pinto YM, Liao R, Jain MK.** Kruppel-like factor 15 is a regulator of cardiomyocyte hypertrophy. *Proc Natl Acad Sci USA* 104: 7074–7079, 2007.
13. **Freerksen DL, Hartzell CR.** Glucocorticoid stimulation of metabolism and glycerol-3-phosphate dehydrogenase activity in cultured heart cells. *J Cell Physiol* 126: 206–210, 1986.
14. **Gardner DG, Wu JP, LaPointe MC, Hedges BK, Deschepper CF.** Expression of the gene for the atrial natriuretic peptide in cardiac myocytes in vitro. *Cardiovasc Drugs Ther* 2: 479–486, 1988.
15. **Gray S, Feinberg MW, Hull S, Kuo CT, Watanabe M, Sen-Banerjee S, DePina A, Haspel R, Jain MK.** The Kruppel-like factor KLF15 regulates the insulin-sensitive glucose transporter GLUT4. *J Biol Chem* 277: 34322–34328, 2002.
16. **Guder G, Bauersachs J, Frantz S, Weismann D, Allolio B, Ertl G, Angermann CE, Stork S.** Complementary and incremental mortality risk prediction by cortisol and aldosterone in chronic heart failure. *Circulation* 115: 1754–1761, 2007.
17. **Honer C, Nam K, Fink C, Marshall P, Ksander G, Chatelain RE, Cornell W, Steele R, Schweitzer R, Schumacher C.** Glucocorticoid receptor antagonism by cyproterone acetate and RU486. *Mol Pharmacol* 63: 1012–1020, 2003.
18. **Hutson SM, Sweatt AJ, Lanoue KF.** Branched-chain [corrected] amino acid metabolism: implications for establishing safe intakes. *J Nutr* 135: 1557S–1564S, 2005.
19. **Iwatani S, Van Dien S, Shimbo K, Kubota K, Kageyama N, Iwahata D, Miyano H, Hirayama K, Usuda Y, Shimizu K, Matsui K.** Determination of metabolic flux changes during fed-batch cultivation from measurements of intracellular amino acids by LC-MS/MS. *J Biotechn* 128: 93–111, 2007.
20. **James CG, Ulici V, Tuckermann J, Underhill TM, Beier F.** Expression profiling of dexamethasone-treated primary chondrocytes identifies targets of glucocorticoid signalling in endochondral bone development. *BMC Genomics* 8: 205, 2007.
21. **Kanda F, Okuda S, Matsushita T, Takatani K, Kimura KI, Chihara K.** Steroid myopathy: pathogenesis and effects of growth hormone and insulin-like growth factor-I administration. *Horm Res* 56, *Suppl* 1: 24–28, 2001.
22. **Kniss DA, Burry RW.** Glucocorticoid hormones inhibit DNA synthesis in glial cells cultured in chemically defined medium. *Exp Cell Res* 161: 29–40, 1985.
23. **Kodde IF, van der Stok J, Smolenski RT, de Jong JW.** Metabolic and genetic regulation of cardiac energy substrate preference. *Comp Biochem Physiol* 146: 26–39, 2007.
24. **Komamura K, Shirotani-Ikejima H, Tatsumi R, Tsujita-Kuroda Y, Kitakaze M, Miyatake K, Sunagawa K, Miyata T.** Differential gene expression in the rat skeletal and heart muscle in glucocorticoid-induced myopathy: analysis by microarray. *Cardiovasc Drugs Ther* 17: 303–310, 2003.
25. **Kurowski TT, Czerwinski SM.** Glucocorticoid modulation of cardiac mass and protein. *Med Sci Sports Exerc* 22: 312–315, 1990.
26. **La Mear NS, MacGilvray SS, Myers TF.** Dexamethasone-induced myocardial hypertrophy in neonatal rats. *Biol Neonate* 72: 175–180, 1997.
27. **Lefer AM.** Influence of corticosteroids on mechanical performance of isolated rat papillary muscles. *Am J Physiol* 21: 518–524, 1968.
28. **Lister K, Autelitano DJ, Jenkins A, Hannan RD, Sheppard KE.** Cross talk between corticosteroids and alpha-adrenergic signalling augments cardiomyocyte hypertrophy: a possible role for SGK1. *Cardiovasc Res* 70: 555–565, 2006.
29. **Liu SF, Newton R, Evans TW, Barnes PJ.** Differential regulation of cyclo-oxygenase-1 and cyclo-oxygenase-2 gene expression by lipopolysaccharide treatment in vivo in the rat. *Clin Sci (Lond)* 90: 301–306, 1996.
30. **Menconi M, Fareed M, O'Neal P, Poylin V, Wei W, Hasselgren PO.** Role of glucocorticoids in the molecular regulation of muscle wasting. *Crit Care Med* 35: S602–S608, 2007.
31. **Mendez M, LaPointe MC.** Trophic effects of the cyclooxygenase-2 product prostaglandin E(2) in cardiac myocytes. *Hypertension* 39: 382–388, 2002.
32. **Miller AL, Webb MS, Thompson EB.** Comparison of two structurally diverse glucocorticoid receptor agonists: cortivazol selectively regulates a distinct set of genes separate from dexamethasone in CEM cells. *Steroids* 72: 673–681, 2007.
33. **Narayanan N, Yang C, Xu A.** Dexamethasone treatment improves sarcoplasmic reticulum function and contractile performance in aged myocardium. *Mol Cell Biochem* 266: 31–36, 2004.
34. **Pazirandeh A, Xue Y, Prestegaard T, Jondal M, Okret S.** Effects of altered glucocorticoid sensitivity in the T cell lineage on thymocyte and T cell homeostasis. *Faseb J* 16: 727–729, 2002.
35. **Penefsky ZJ, Kahn M.** Inotropic effects of dexamethasone in mammalian heart muscle. *Eur J Pharmacol* 15: 259–266, 1971.
36. **Phuc Le P, Friedman JR, Schug J, Brestelli JE, Parker JB, Bochkis IM, Kaestner KH.** Glucocorticoid receptor-dependent gene regulatory networks (Abstract). *PLoS Genet* 1: e16, 2005.
37. **Rhen T, Cidlowski JA.** Antiinflammatory action of glucocorticoids–new mechanisms for old drugs. *N Engl J Med* 353: 1711–1723, 2005.
38. **Rupprecht R, Arriza JL, Spengler D, Reul JM, Evans RM, Holsboer F, Damm K.** Transactivation and synergistic properties of the mineralocorticoid receptor: relationship to the glucocorticoid receptor. *Mol Endocrinol* 7: 597–603, 1993.
39. **Sainte-Marie Y, Nguyen Dinh Cat A, Perrier R, Mangin L, Soukaseum C, Peuchmaur M, Tronche F, Farman N, Escoubet B, Benitah JP, Jaisser F.** Conditional glucocorticoid receptor expression in the heart induces atrio-ventricular block. *FASEB J* 21: 3133–3141, 2007.
40. **Sano M, Tokudome S, Shimizu N, Yoshikawa N, Ogawa C, Shirakawa K, Endo J, Katayama T, Yuasa S, Ieda M, Makino S, Hattori F, Tanaka H, Fukuda K.** Intramolecular control of protein stability, subnuclear compartmentalization, and coactivator function of peroxisome proliferator-activated receptor gamma coactivator 1alpha. *J Biol Chem* 282: 25970–25980, 2007.
41. **Schlechte JA, Schmidt TJ.** Use of [3H]cortivazol to characterize glucocorticoid receptors in a dexamethasone-resistant human leukemic cell line. *J Clin Endocrinol Metab* 64: 441–446, 1987.

42. **Schulz R, Nava E, Moncada S.** Induction and potential biological relevance of a Ca(2+)-independent nitric oxide synthase in the myocardium. *Br J Pharmacol* 105: 575–580, 1992.
43. **She P, Reid TM, Bronson SK, Vary TC, Hajnal A, Lynch CJ, Hutson SM.** Disruption of BCATm in mice leads to increased energy expenditure associated with the activation of a futile protein turnover cycle. *Cell Metab* 6: 181–194, 2007.
44. **Shimizu N, Ouchida R, Yoshikawa N, Hisada T, Watanabe H, Okamoto K, Kusuhara M, Handa H, Morimoto C, Tanaka H.** HEXIM1 forms a transcriptionally abortive complex with glucocorticoid receptor without involving 7SK RNA and positive transcription elongation factor b. *Proc Natl Acad Sci USA* 102: 8555–8560, 2005.
45. **Stojadinovic O, Lee B, Vouthounis C, Vukelic S, Pastar I, Blumenberg M, Brem H, Tomic-Canic M.** Novel genomic effects of glucocorticoids in epidermal keratinocytes: inhibition of apoptosis, interferon-gamma pathway, and wound healing along with promotion of terminal differentiation. *J Biol Chem* 282: 4021–4034, 2007.
46. **Sun H, Sheveleva E, Xu B, Inoue H, Bowden TG, Chen QM.** Corticosteroids induce COX-2 expression in cardiomyocytes: role of glucocorticoid receptor and C/EBP-β. *Am J Physiol Cell Physiol* 295: C915–C922, 2008.
47. **Testa M, Rocca B, Spath L, Ranelletti FO, Petrucci G, Ciabattoni G, Naro F, Schiaffino S, Volpe M, Reggiani C.** Expression and activity of cyclooxygenase isoforms in skeletal muscles and myocardium of humans and rodents. *J Appl Physiol* 103: 1412–1418, 2007.
48. **Walker BR.** Glucocorticoids and cardiovascular disease. *Eur J Endocrinol* 157: 545–559, 2007.
49. **Wang JC, Shah N, Pantoja C, Meijsing SH, Ho JD, Scanlan TS, Yamamoto KR.** Novel arylpyrazole compounds selectively modulate glucocorticoid receptor regulatory activity. *Genes Dev* 20: 689–699, 2006.
50. **Wang L, Feng ZP, Duff HJ.** Glucocorticoid regulation of cardiac K+ currents and L-type Ca2+ current in neonatal mice. *Circ Res* 85: 168–173, 1999.
51. **Whitehurst RM Jr, Zhang M, Bhattacharjee A, Li M.** Dexamethasone-induced hypertrophy in rat neonatal cardiac myocytes involves an elevated L-type Ca(2+)current. *J Mol Cell Cardiol* 31: 1551–1558, 1999.
52. **Yoshikawa N, Makino Y, Okamoto K, Morimoto C, Makino I, Tanaka H.** Distinct interaction of cortivazol with the ligand binding domain confers glucocorticoid receptor specificity: cortivazol is a specific ligand for the glucocorticoid receptor. *J Biol Chem* 277: 5529–5540, 2002.
53. **Yoshikawa N, Yamamoto K, Shimizu N, Yamada S, Morimoto C, Tanaka H.** The distinct agonistic properties of the phenylpyrazolosteroid cortivazol reveal interdomain communication within the glucocorticoid receptor. *Mol Endocrinol* 19: 1110–1124, 2005.

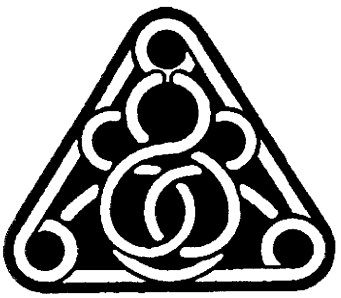

Renal Damage Inhibited in Mice Lacking Angiotensinogen Gene Subjected to Unilateral Ureteral Obstruction

Yasumitsu Uchida, Akira Miyajima, Eiji Kikuchi, Norihide Kozakai, Takeo Kosaka, Masaki Ieda, Keiichi Fukuda, Takashi Ohigashi, and Mototsugu Oya

OBJECTIVES To determine how angiotensin II (Ang II) contributes to renal interstitial fibrosis, the inflammatory response, and tubular cell apoptosis and proliferation in unilateral ureteral obstruction using mice genetically deficient in angiotensinogen ($Agt^{-/-}$).

METHODS The left kidney of wild-type mice (WT; C57BL/6) and $Agt^{-/-}$ mice was obstructed for 2 weeks, and then both kidneys were harvested. The serum Ang II levels were determined by radioimmunoassay. The expression of transforming growth factor-β in renal tissue was assessed using enzyme-linked immunosorbent assay. The renal tissue was stained with Masson's trichrome. Renal tubular proliferation and apoptosis was detected by immunostaining for proliferating cell nuclear antigen and single-stranded DNA, respectively. Interstitial leukocyte and macrophage infiltration was investigated by immunostaining for CD45 and F4/80, respectively.

RESULTS The serum Ang II levels in the $Agt^{-/-}$ mice were significantly lower than those in the WT mice ($P < .01$), and tissue transforming growth factor-β in the obstructed kidney of $Agt^{-/-}$ mice was significantly lower than that in WT mice ($P < .05$). Interstitial collagen deposition was significantly lower in the $Agt^{-/-}$ obstructed kidneys than in the WT obstructed kidneys ($P < .01$). Tubular proliferation was significantly greater and tubular apoptosis was significantly lower in the $Agt^{-/-}$ obstructed kidneys than in the WT obstructed kidneys ($P < .01$ and $P < .01$, respectively). Interstitial infiltration by leukocytes and macrophages was significantly lower in the $Agt^{-/-}$ obstructed kidneys than in the WT obstructed kidneys ($P < .01$ and $P < .01$, respectively).

CONCLUSIONS The results of the present study support the targeting of Ang II as a reasonable approach by which to prevent renal tissue damage in unilateral ureteral obstruction. UROLOGY 74: 938–943, 2009. © 2009 Elsevier Inc.

Angiotensin II (Ang II) has been shown to be involved in the pathophysiologic changes in experimental models of tubulointerstitial fibrosis, including unilateral ureteral obstruction (UUO).[1] Ang II is a potent inducer of transforming growth factor-β (TGF-β) in several cell types, such as tubular epithelial cells and mesangial cells.[2-4] We previously confirmed that Ang II significantly increased TGF-β in normal rat kidney 52E cells.[5] Morrissey et al.[6] used an Ang II receptor blocker and Ang II-converting enzyme inhibitor in UUO, which resulted in a decrease in interstitial fibrosis accompanied by a decrease in TGF-β. Therefore, the Ang II-TGF-β pathway is important for understanding the pathophysiologic mechanism of tubulointerstitial fibrosis in UUO.

Approximately 80% of the kidney volume is occupied by the renal tubules,[7] and a positive correlation has been found between the histologic presence of tubular atrophy and a decreased glomerular filtration rate in glomerulonephritis.[8] In UUO, it has been suggested that renal tubular apoptosis is related to renal tissue loss and dysfunction.[9] Accordingly, it is important to focus on the renal tubular damage in UUO. We have previously reported that TGF-β may play a role in renal tubular cell apoptosis in UUO.[5] Newly generated mice genetically deficient in angiotensinogen ($Agt^{-/-}$) can be used to study the role of Ang II, which exists upstream of TGF-β, in the inflammatory damage in the obstructed kidney. The present study was undertaken to determine how Ang II contributes to renal interstitial fibrosis, inflammatory responses, and tubular cell apoptosis and proliferation using $Agt^{-/-}$ mice.

From the Departments of Urology and Regenerative Medicine and Advanced Cardiac Therapeutics, Keio University School of Medicine; and Department of Urology, International University of Health and Welfare, Mita Hospital, Tokyo, Japan

Reprint requests: Akira Miyajima, M.D., Department of Urology, Keio University School of Medicine, 35 Shinanomachi, Shinjuku-ku, Tokyo, Japan. E-mail: akiram@sc.itc.keio.ac.jp

Submitted: September 29, 2008, accepted (with revisions): February 26, 2009

0090-4295/09/$34.00
doi:10.1016/j.urology.2009.02.059

MATERIAL AND METHODS

Experimental Design

Female wild-type (WT; C57BL/6) and angiotensinogen knockout ($Agt^{-/-}$) mice (n = 10/group) generated as previously described[10,11] were used at 8 weeks of age. The UUO model was created with the mice under intraperitoneal pentobarbital-induced anesthesia. The left ureter was ligated with silk 4-0 suture through an abdominal midline incision under sterile conditions. The obstructed and unobstructed kidneys were harvested after intraperitoneal pentobarbital administration at day 14. The mice were handled according to approved institutional guidelines.

Measurement of Serum Angiotensin II

Peripheral blood was collected by retro-orbital venous plexus puncture, and the serum Ang II concentration was measured by radioimmunoassay (Mitsubishi Kagaku BCL, Tokyo, Japan).

Tissue TGF-β Assay

The harvested kidneys were hemisected, weighed, and homogenized with acid-ethanol (90% EtOH in 0.2 M HCl: 45 mL of 100% EtOH, 1 mL of 10 M HCl, and 4 mL of water). The samples were maintained for 24 hours at 4°C. The water was volatilized with an evaporator. The samples were resuspended in 0.7-1 mL of Dulbecco's modified Eagle's medium containing 0.1% bovine serum albumin, vortexed, and centrifuged at 8000 rpm for 30 minutes. The supernatant was transferred to another tube. After equilibration at neutral pH with 1 N NaOH, the samples were filtered, collected, and assayed for TGF-β by enzyme-linked immunosorbent assay using a Quantikine assay kit (MB100B, R&D Systems, Minneapolis, MN). The results were normalized and are expressed as ng/mg tissue TGF-β.

Determination of Interstitial Collagen Deposition

The slides were stained with Masson's trichrome. For each section, 10 fields were digitized and scanned at 200× magnification using imaging software (Photoshop, Adobe, San Jose, CA). The number of points overlapping the blue collagen staining was counted using a grid superimposed on the image.

Immunohistochemistry to Stain CD45, F4/80, Single-Stranded DNA, and Proliferating Cell Nuclear Antigen

Wedges of hemisected obstructed and contralateral kidneys were placed in 10% formalin and embedded in paraffin. Paraffin-embedded sections (4 μm) were cut onto glass slides. The sections were dewaxed in xylene, rehydrated in decreasing concentrations of ethanol, and washed 3 times in phosphate-buffered saline for 10 minutes. Endogenous peroxidase was quenched for 45 minutes with a 0.6% methanol solution. After washing in filtered water and phosphate-buffered saline, a blocking step was included using 1% bovine serum albumin plus avidin and biotin blocking solutions (Vector Kit, Vector Laboratories, Burlingame, CA) for 30 minutes. Primary antibody (polyclonal anti-CD45 antibody, Santa Cruz Biotechnology, Santa Cruz, CA; polyclonal antiproliferating cell nuclear antigen [PCNA] antibody, Santa Cruz Biotechnology; monoclonal anti-F4/80 antibody, Serotec, Oxford, UK; and polyclonal anti-single-stranded DNA [ssDNA] antibody, Dako, Glostrup, Denmark) was then applied at room temperature for 1 hour. Diluted biotinylated secondary antibody (Vector Laboratories) was applied for 30 minutes. The sections were then incubated with avidin-biotin peroxidase complex (Vector Laboratories) and developed with diaminobenzidine. The slides were washed and counterstained with 10% hematoxylin for 1-2 minutes. Positive PCNA and ssDNA cells from renal tubules were counted in 10 high-power fields (HPFs) at 400× magnification by 2 independent investigators unaware of the which kidney was with which group. Positive interstitium CD45 cells and F4/80 cells were evaluated in the same manner as that for PCNA and ssDNA.

Statistical Analysis

All results are expressed as the mean ± SD and were analyzed for significance by one-way analysis of variance and multiple comparison tests.

RESULTS

Measurement of Serum Ang II

First, the Ang II concentrations in serum were measured with radioimmunoassay to confirm whether Ang II was detected in $Agt^{-/-}$ mice. The serum concentration of Ang II in $Agt^{-/-}$ mice was lower than the lower limit of detection (<10.0 ± 0.0 pg/mL, n = 10). In contrast, serum Ang II was detected in the WT mice (159.3 ± 62.0 pg/mL, n = 10, $P < .01$).

Measurement of Tissue TGF-β Concentration in Mice With UUO

Next, to confirm whether renal tissue TGF-β in $Agt^{-/-}$ mice was affected, we measured the TGF-β concentration in kidney tissue, using an enzyme-linked immunosorbent assay (Table 1). The tissue TGF-β content in the unobstructed kidneys in the $Agt^{-/-}$ mice was slightly lower than that in the unobstructed kidneys in WT mice, although the difference was not statistically significant ($P = .1252$). However, the tissue TGF-β content in the obstructed kidneys in the $Agt^{-/-}$ mice was significantly lower than that in the obstructed kidneys in the WT mice ($P < .05$). Furthermore, although the tissue TGF-β content in the obstructed kidneys was significantly greater than that in the unobstructed kidneys in WT mice (105.2 ± 51.6 vs 27.1 ± 16.3 pg/mg tissue, respectively; $P < .01$), no statistically significant difference was found in the $Agt^{-/-}$ mice (37.1 ± 29.2 vs 11.5 ± 5.7 pg/mg tissue, respectively; $P = .072$).

Interstitial Collagen Deposition in UUO

To determine the difference between the WT mice and $Agt^{-/-}$ mice with interstitial fibrosis in UUO, we stained the slides with Masson's trichrome and determined the blue-stained collagen deposition (Table 1). UUO resulted in a marked accumulation of interstitial collagen compared with the contralateral unobstructed kidneys in WT mice (19.8% ± 4.3% vs 2.4% ± 1.8%, respectively; $P < .0001$). The same effect was seen in the $Agt^{-/-}$ mice (8.3% ± 2.1% vs 1.2% ± 1.2% for obstructed vs unobstructed, respectively; $P < .0001$). However, the interstitial collagen deposition in the obstructed kidneys in the

Table 1. Tissue TGF-β concentration and positive interstitial collagen deposition, CD45, F4/80 cells, ssDNA, and PCNA nuclei

Group	TGF-β (pg/mg tissue)	Collagen Deposition (%/HPF)	CD45 (Positive Cells/HPF)	F4/80 (Positive Cells/HPF)	ssDNA (Tubular Nuclei/HPF)	PCNA (Tubular Nuclei/HPF)
WT (n = 10)						
Obstructed	105.2 ± 51.6*	19.8 ± 4.3†	24.6 ± 5.4†	26.3 ± 5.3†	45.0 ± 6.6†	15.2 ± 3.3†
Unobstructed	27.1 ± 16.3	2.4 ± 1.8	1.4 ± 1.0	1.4 ± 1.1	0.3 ± 0.5	3.6 ± 1.3
$Agt^{-/-}$ (n = 10)						
Obstructed	37.1 ± 29.2‡	8.3 ± 2.1†§	11.8 ± 2.6†§	11.2 ± 3.7*§	24.8 ± 5.0†§	26.2 ± 5.3*§
Unobstructed	11.5 ± 5.7	1.2 ± 1.2	0.3 ± 0.5	2.2 ± 1.7	0.2 ± 0.4	5.0 ± 2.0

TGF-β = transforming growth factor-β; ssDNA = single-stranded DNA; PCNA = proliferating cell nuclear antigen; WT = wild type; $Agt^{-/-}$ = angiotensinogen deficient.
* $P < .01$ compared with unobstructed counterpart.
† $P < .0001$ compared with unobstructed counterpart.
‡ $P < .01$ compared with obstructed kidney of WT mice.
§ $P < .05$ compared with obstructed kidney of WT mice.

$Agt^{-/-}$ mice was significantly lower than in the obstructed kidneys in the WT mice ($P < .01$; Fig. 1A,B). No difference in interstitial collagen deposition was observed in the unobstructed kidneys of either group.

Detection of Interstitial Leukocyte and Macrophage Infiltration in UUO

We also investigated the inflammatory changes in UUO. Leukocyte infiltration was evaluated by immunostaining for CD45, and macrophage infiltration was evaluated by immunostaining for F4/80. The obstructed kidneys had significantly greater leukocyte and macrophage infiltration compared with the unobstructed kidneys in the WT mice (24.6 ± 5.5 and 26.3 ± 5.3 vs 1.4 ± 1.0 and 1.4 ± 1.1 cells/HPF, respectively; $P < .0001$; Table 1). The same effect was seen in the $Agt^{-/-}$ mice, with corresponding values of 11.8 ± 2.6 and 11.2 ± 3.7 vs 0.3 ± 0.5 and 2.2 ± 1.7 cells/HPF ($P < .0001$ and $P < .01$, respectively; Table 1). The obstructed kidneys in the $Agt^{-/-}$ mice had significantly lower leukocyte and macrophage infiltration than did the obstructed kidneys in the WT mice ($P < .01$ and $P < .01$, respectively; Table 1 and Fig. 1C-F). No differences were found in interstitial leukocyte infiltration and macrophage infiltration in the unobstructed kidneys of both groups.

Apoptosis in UUO

To determine renal tubular apoptosis, ssDNA immunostaining was performed in paraffin-embedded sections. The obstructed kidneys had significantly greater tubular apoptosis than the unobstructed kidneys of the WT mice (45.0 ± 6.6 vs 0.3 ± 0.5 nuclei/HPF, respectively; $P < .0001$; Table 1). The difference between the obstructed and unobstructed kidneys was apparent from the apoptotic cell counts. The same effect was seen in the $Agt^{-/-}$ mice, with corresponding values of 24.8 ± 5.0 vs 0.2 ± 0.4 nuclei/HPF ($P < .0001$; Table 1). However, tubular apoptosis was significantly lower in the obstructed kidneys of the $Agt^{-/-}$ mice than in the obstructed kidneys of the WT mice ($P < .01$; Table 1 and Fig. 1G,H). No difference was found in tubular apoptosis in the unobstructed kidneys between the 2 groups.

Tubular Proliferation in UUO

We next examined renal proliferation by immunostaining for PCNA. In the WT and $Agt^{-/-}$ mice, renal tubules in the obstructed kidneys showed significantly more proliferation (15.2 ± 3.3 and 26.2 ± 5.3 nuclei/HPF, respectively) than did the unobstructed kidneys (3.6 ± 1.3 and 5.0 ± 2.0 nuclei/HPF; $P < .0001$ and $P < .01$, respectively; Table 1). No significant difference was found in tubular proliferation in the unobstructed kidneys between the 2 groups, although the tubular proliferation was significantly greater in the obstructed kidneys in the $Agt^{-/-}$ mice than in the WT mice ($P < .01$; Table 1 and Fig. 1I,J).

COMMENT

Ang II has been considered an important factor in UUO.[12,13] Several animal studies of UUO have demonstrated that drugs such as Ang II receptor antagonists[6,14-16] and angiotensin-converting enzyme inhibitors,[6,17] used clinically for hypertension, ameliorate UUO-induced renal interstitial fibrosis by inhibiting hormonal signaling. This downregulation of hormonal signaling results in TGF-β inhibition, subsequent to inhibiting interstitial fibrosis. TGF-β has been reported to exert its action directly by stimulating the synthesis of extracellular matrix components and reducing collagenase production or indirectly through other profibrogenic factors, such as connective tissue growth factor, involving Smad proteins.[18]

Fern et al.[19] reported that angiotensinogen expression is related to renal interstitial fibrosis in UUO using neonatal mice. However, few studies of UUO using mature mice lacking the angiotensinogen gene to delete Ang II have been done, and the renal inflammatory responses in the various studies have been different. On the basis of the concept that renal tissue injury by UUO is promoted by Ang II, the study of mice lacking the angiotensinogen gene might help elucidate the role of Ang II in renal

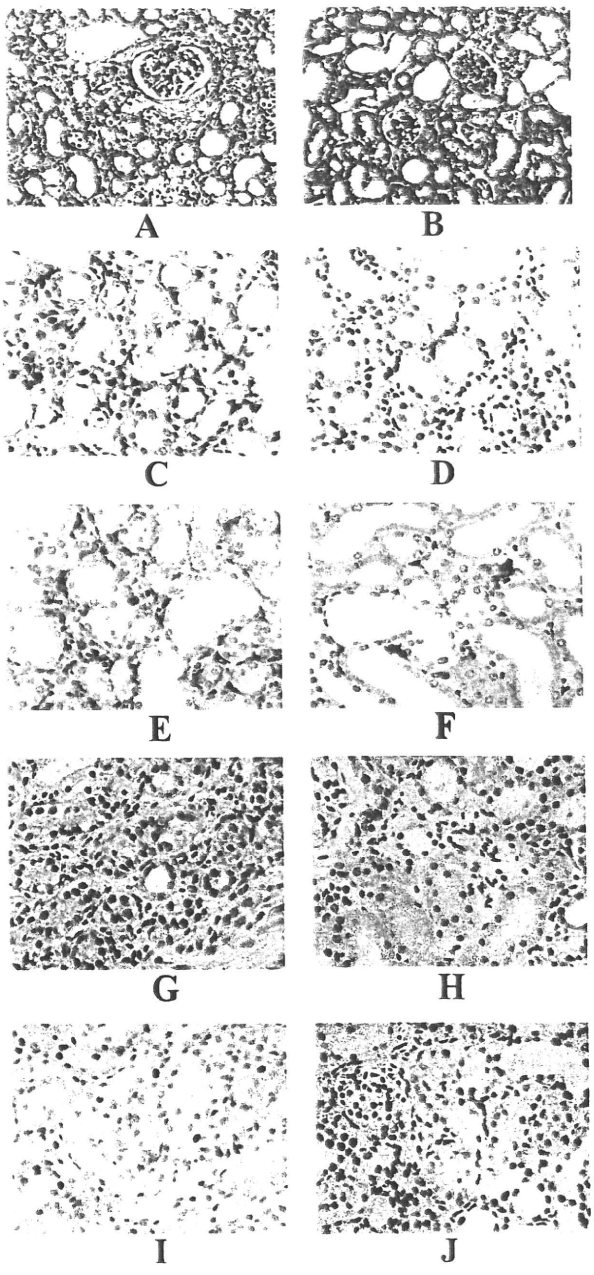

Figure 1. Interstitial fibrosis detected by Masson's trichrome staining (200×). **(A)** Wild-type (WT) obstructed kidney and **(B)** angiotensinogen-deficient ($Agt^{-/-}$) obstructed kidney showing leukocyte infiltrations detected by immunostaining for CD45 (400×). **(C)** WT obstructed kidney and **(D)** $Agt^{-/-}$ obstructed kidney showing macrophage infiltration detected by immunostaining for F4/80 (400×). **(E)** WT obstructed kidney and **(F)** $Agt^{-/-}$ obstructed kidney showing tubular apoptosis detected by immunostaining for single-stranded DNA (400×). **(G)** WT obstructed kidney and **(H)** $Agt^{-/-}$ obstructed kidney showing tubular proliferation detected by immunostaining for proliferating cell nuclear antigen (400×). **(I)** WT obstructed kidney and **(J)** $Agt^{-/-}$ obstructed kidney.

tubular damage and interstitial fibrosis of UUO. Therefore, we sought to confirm the underlying effects of Ang II on renal tubular damage and interstitial fibrosis in UUO by comparing mice lacking the angiotensinogen gene ($Agt^{-/-}$) and WT mice.

Although Ang II basically induces fibrosis through TGF-β signaling,[2-4,6] it has been reported that TGF-β stimulates angiotensinogen gene expression, at least in proximal tubular cells, suggesting that a positive feedback loop further enhances renal injury.[20] Our data have shown that the serum concentration of Ang II in $Agt^{-/-}$ mice was less than the lower limit of detection, and, accordingly, the tissue TGF-β increase in the obstructed kidneys was significantly inhibited in the $Agt^{-/-}$ mice, a finding that was not significantly different from that in the $Agt^{-/-}$ contralateral unobstructed kidneys. This implies that Ang II exists upstream of TGF-β and that Ang II plays an important role in TGF-β induction. Nevertheless, TGF-β was not completely inhibited in the obstructed kidneys of the $Agt^{-/-}$ mice, as we observed a complete reduction of serum Ang II in the $Agt^{-/-}$ mice. Taken together, these findings seem to indicate that Ang II is partly involved in TGF-β induction because the TGF-β inhibition in the $Agt^{-/-}$ UUO model was moderate.

Because TGF-β is known to be a pro-fibrotic and pro-apoptotic cytokine,[5,21] we investigated how these cellular events were affected by UUO in $Agt^{-/-}$ mice. Our results showed that renal interstitial fibrosis was significantly lower in the obstructed kidneys of $Agt^{-/-}$ mice compared with those in WT mice and that tubular apoptosis was significantly lower and tubular proliferation significantly greater in the obstructed kidneys of $Agt^{-/-}$ mice compared with the levels in the obstructed kidneys of WT mice. These results suggest that the Ang II-TGF-β pathway is a key player in the development of these cellular events in UUO.

TGF-β has long been known to have anti-inflammatory properties. Mice lacking the TGF-β gene die with multiorgan inflammation, along with other effects, including overexpression of adhesion molecules.[22] However, the response to TGF-β might depend on a variety of factors. Koyanagi et al.[23] reported that a monoclonal antibody to TGF-β1 blocked the cardiac inflammation induced by chronic inhibition of nitric oxide synthesis with N^{ω}-nitro-L-arginine methylester, suggesting a pro-inflammatory role for TGF-β or its downstream mediators. El Chaar et al.[17] demonstrated that 1D11, a monoclonal antibody that is active against all 3 isoforms of TGF-β, significantly decreased macrophage infiltration into the kidneys of UUO, suggesting that TGF-β contributes to the inflammatory effect in UUO. However, it remains controversial whether TGF-β promotes or inhibits an inflammatory response. Our results showed that renal interstitial infiltration of leukocytes and macrophages in the obstructed kidneys was significantly lower in $Agt^{-/-}$ mice compared with WT mice. Therefore, the UUO-induced inflammatory changes in the obstructed kidney were inhibited in $Agt^{-/-}$ mice compared with those in WT mice. These findings suggest that the Ang

II-TGF-β pathway may exert a progressive effect on the inflammatory response in UUO.

Explaining the mechanism of renal injury by the Ang II-TGF-β pathway using our results appears insufficient, because TGF-β is not differentially regulated in the setting of UUO in $Agt^{-/-}$ animals. It has been reported for other pathways that Ang II, by way of the Ang II type 1 receptor, activates the Smad signaling system and the Rho/Rho kinase pathway that upregulates connective tissue growth factor production and results in renal fibrosis not mediated by the Ang II-TGF-β pathway.[24] Furthermore, it was reported that Ang II by way of the Ang II type 1 receptor and Ang II type 2 receptor activates the nuclear factor (NF)-κB pathway and causes inflammatory responses through the regulation of NF-κB[16] and pro-inflammatory genes, such as several chemokines or adhesion molecules.[24] We have previously demonstrated that dehydroxymethylepoxyquinomicin, an NF-κB activation inhibitor, did not affect TGF-β activity in the obstructed kidneys of UUO but did ameliorate interstitial fibrosis, tubular apoptosis, and leukocyte infiltration, suggesting that the NF-κB pathway seems to be substantially associated with downstream TGF-β-induced cellular events in UUO.[25] It is conceivable that Ang II is involved in the renal morphologic events of UUO in a way that could be either dependent on, or independent of, the TGF-β pathway.

Of particular interest is the result that interstitial fibrosis and tubular apoptosis occurred in $Agt^{-/-}$ mice, despite the loss of Ang II. Factors other than the Ang II pathway may be implicated in these events, as described in our report. It is believed that these changes are induced by intrarenal pressure and result in tubular cell stretch and the release of other mediators.[26,27] Nevertheless, the cause of the fibrosis or apoptosis in the obstructed kidneys of $Agt^{-/-}$ mice is unknown and remains to be elucidated.

When a patient presents with an obstructed kidney, the patient should be treated as soon as the obstruction has been detected. However, a considerable period can elapse between the diagnosis and relief of the obstruction; furthermore, renal damage is not immediately reversed by relieving the obstruction. Additionally, prolonged obstruction leads to irreversible renal dysfunction. It would be very useful if the renal damage and renal dysfunction could be prevented by pharmacologic agents until the obstruction could be ameliorated. Additional analysis targeting Ang II is required.

CONCLUSIONS

Our results have indicated that targeted deletion of the Agt gene results in inhibition of renal tissue TGF-β, followed by inhibition of fibrotic and renal tubular apoptosis, and inhibition of the inflammatory response in the obstructed kidneys of mice subjected to UUO. The results of the present study support the targeting of Ang II as a reasonable approach to prevent renal tissue damage in UUO.

Acknowledgment. To Susumu Tominaga, Takako Asano, and Kaori Seta of the National Defense Medical College for their excellent technical assistance.

References

1. Klahr S, Morrissey JJ. Angiotensin II and gene expression in the kidney. *Am J Kidney Dis.* 1998;31:171-176.
2. Wolf G, Mueller E, Stahl RA, et al. Angiotensin II-induced hypertrophy of cultured murine proximal tubular cells is mediated by endogenous transforming growth factor-beta. *J Clin Invest.* 1993; 92:1366-1372.
3. Wolf G. Angiotensin II is involved in the progression of renal disease: importance of non-hemodynamic mechanism. *Nephrologie.* 1998;19:451-456.
4. Ardaillou R, Chansel D, Chatziantoniou C, et al. Mesangial AT1 receptors: expression, signaling, and regulation. *J Am Soc Nephrol.* 1999;10(suppl 11):S40-S46.
5. Miyajima A, Chen J, Lawrence C, et al. Antibody to transforming growth factor-beta ameliorates tubular apoptosis in unilateral ureteral obstruction. *Kidney Int.* 2000;58:2301-2313.
6. Morrissey JJ, Ishidoya S, McCracken R, et al. Nitric oxide generation ameliorates the tubulointerstitial fibrosis of obstructive nephropathy. *J Am Soc Nephrol.* 1996;7:2202-2212.
7. Eddy AA. Experimental insights into the tubulointerstitial disease accompanying primary glomerular lesions. *J Am Soc Nephrol.* 1994; 5:1273-1287.
8. Risdon RA, Sloper JC, De Wardener HE. Relationship between renal function and histological changes found in renal-biopsy specimens from patients with persistent glomerular nephritis. *Lancet.* 1968;2:363-366.
9. Truong LD, Petrusevska G, Yang G, et al. Cell apoptosis and proliferation in experimental chronic obstructive uropathy. *Kidney Int.* 1996;50:200-207.
10. Ieda M, Fukuda K, Hisaka Y, et al. Endothelin-1 regulates cardiac sympathetic innervation in the rodent heart by controlling nerve growth factor expression. *J Clin Invest.* 2004;113:876-884.
11. Tanimoto K, Sugiyama F, Goto Y, et al. Angiotensinogen-deficient mice with hypotension. *J Biol Chem.* 1994;269:31334-31337.
12. Gulmi F, Felsen D, Vaughan EJ. Pathophysiology of urinary tract obstruction. In: Walsh PC, Retik AB, Vaughan ED Jr, et al., editors. *Campbell's Urology*, 8th ed. Philadelphia: WB Saunders; 2002:443-444.
13. Klahr S, Morrissey JJ. Obstructive nephropathy and renal fibrosis. *Am J Physiol Renal Physiol.* 2002;283:F861-F875.
14. Ishidoya S, Morrissey JJ, McCracken R, et al. Angiotensin II receptor antagonist ameliorates renal tubulointerstitial fibrosis caused by unilateral ureteral obstruction. *Kidney Int.* 1995;47:1285-1294.
15. Morrissey JJ, Klahr S. Effect of AT2 receptor blockade on the pathogenesis of renal fibrosis. *Am J Physiol.* 1999;276:F39-F45.
16. Esteban V, Ruperez M, Vita JR, et al. Effect of simultaneous blockade of AT1 and AT2 receptors on the NFkappaB pathway and renal inflammatory response. *Kidney Int Suppl.* 2003;86:S33-S38.
17. El Chaar M, Chen J, Seshan SV, et al. Effect of combination therapy with enalapril and the TGF-beta antagonist 1D11 in unilateral ureteral obstruction. *Am J Physiol Renal Physiol.* 2007;292: F1291-F1301.
18. Wolf G. Renal injury due to renin-angiotensin-aldosterone system activation of the transforming growth factor-β pathway. *Kidney Int.* 2006;70:1914-1919.
19. Fern RJ, Yesko CM, Thornhill BA, et al. Reduced angiotensinogen expression attenuates renal interstitial fibrosis in obstructive nephropathy in mice. *J Clin Invest.* 1999;103:39-46.
20. Brezniceanu ML, Wei CC, Zhang SL, et al. Transforming growth factor-beta 1 stimulates angiotensinogen gene expression in kidney proximal tubular cells. *Kidney Int.* 2006;69:1977-1985.
21. Border WA, Okuda S, Languino L, et al. Suppression of experimental glomerulonephritis by antiserum against transforming growth factor β1. *Nature.* 1990;346:371-374.

22. Letterio JJ, Roberts AB. Regulation of immune responses by TGF-beta. *Annu Rev Immunol.* 1998;16:137-161.
23. Koyanagi M, Egashira K, Kubo-Inoue M, et al. Role of transforming growth factor-beta$_1$ in cardiovascular inflammatory changes induced by chronic inhibition of nitric oxide synthesis. *Hypertension.* 2000;35:86-90.
24. Ruiz-Ortega M, Ruperez M, Esteban V, et al. Angiotensin II: a key factor in the inflammatory and fibrotic response in kidney diseases. *Nephrol Dial Transplant.* 2006;21:16-20.
25. Miyajima A, Kosaka T, Seta K, et al. Novel nuclear factor kappa B activation inhibitor prevents inflammatory injury in unilateral ureteral obstruction. *J Urol.* 2003;169:1559-1563.
26. Miyajima A, Chen J, Kimman I, et al. Interaction of nitric oxide and transforming growth factor-β1 induced by angiotensin II and mechanical stretch in rat renal tubular epithelial cells. *J Urol.* 2000;164:1729-1734.
27. Miyajima A, Chen J, Poppas DP, et al. Role of nitric oxide in renal tubular apoptosis of unilateral ureteral obstruction. *Kidney Int.* 2001;59:1290-1303.

J Pharmacol Sci 109, 348 - 353 (2009)

Journal of Pharmacological Sciences

Forum Minireview

New Aspects for the Treatment of Cardiac Diseases Based on the Diversity of Functional Controls on Cardiac Muscles: The Regulatory Mechanisms of Cardiac Innervation and Their Critical Roles in Cardiac Performance

Masaki Ieda[1] and Keiichi Fukuda[1,*]

[1]*Department of Regenerative Medicine and Advanced Cardiac Therapeutics, Keio University School of Medicine, 35 Shinanomachi, Shinjuku-ku, Tokyo 160-8582, Japan*

Received October 16, 2008; Accepted November 18, 2008

Abstract. The heart is abundantly innervated, and the nervous system precisely controls the function of this organ. The density of cardiac innervation is altered in diseased hearts, which can lead to unbalanced neural activation and lethal arrhythmia. For example, diabetic sensory neuropathy causes silent myocardial ischemia, characterized by loss of pain perception during myocardial ischemia, and it is a major cause of sudden cardiac death in diabetes mellitus. Despite the clinical importance of cardiac innervation, the mechanisms underlying the control of this process remain poorly understood. We demonstrate that cardiac innervation is determined by the balance between neural chemoattractants and chemorepellents within the heart. Nerve growth factor (NGF), a potent chemoattractant, is synthesized abundantly by cardiomyocytes, and is induced by the upregulation of endothelin-1 during development. By comparison, the neural chemorepellent Sema3a is expressed at high levels in the subendocardium in the early stage of embryogenesis and is downregulated as development progresses, leading to epicardial-to-endocardial transmural sympathetic innervation patterning. We also show that the downregulation of cardiac NGF is a cause of diabetic neuropathy and that NGF supplementation prevents silent myocardial ischemia in diabetes mellitus. Both Sema3a-targeted and Sema3a-overexpressing mice display sudden cardiac death or lethal arrhythmias due to disruption of innervation patterning. The present review focuses on the regulatory mechanisms controlling cardiac innervation and the critical roles of these processes in cardiac performance.

Keywords: cardiac nerve, nerve growth factor, Sema3a, arrhythmia, sudden cardiac death, cardiac disease

Introduction

Cardiac tissues are extensively innervated by autonomic nerves. The sympathetic nervous system produces norepinephrine and increases the heart rate, conduction velocity, as well as myocardial contraction and relaxation. It is well known that sympathetic innervation density, which is high in the subepicardium and the central conduction, is stringently regulated in the heart (1). Regional differences in sympathetic innervation correspond to different areas of influence over cardiac function to effectively control heart rate and myocardial contraction and relaxation. Despite the clinical importance of cardiac innervation, little is known about the developmental and regulatory mechanisms underlying cardiac sympathetic innervation patterning. Moreover, to date there has been no experimental demonstration of the consequences of disrupting this patterning.

The density of cardiac innervation is altered in diseased hearts, as in cases of congestive heart failure and myocardial infarction. Following myocardial injury, cardiac nerves undergo Wallerian degeneration, which may be followed by neurilemmal cell proliferation and axonal regeneration, resulting in heterogeneous innerva-

*Corresponding author. kfukuda@sc.itc.keio.ac.jp
Published online in J-STAGE on March 7, 2009 (in advance)
doi: 10.1254/jphs.08R25FM

tion. Unbalanced sympathetic innervation may trigger lethal arrhythmia through ion channel modulation in cardiomyocytes (2). Also of clinical concern is the development of cardiac sensory denervation in diabetes mellitus (DM) patients. As the sensory nervous system is responsible for pain perception, cardiac sensory denervation can lead to diabetic sensory neuropathy and silent myocardial ischemia. This condition is characterized by loss of pain perception during myocardial ischemia and frequently leads to sudden cardiac death (SCD) in DM patients. Despite the severity of these complications, the molecular mechanisms underlying the control of innervation density in pathological hearts are poorly understood. Addressing these questions requires a better understanding of the anatomical distribution of cardiac nerves and the molecular mechanisms regulating innervation during development.

In this article, we review the regulatory mechanisms involved in neural development in the heart and also discuss the critical role of innervation patterning in cardiac performance.

Cardiac nerve development

Neural crest cells migrate and form sympathetic ganglia by mid-gestation and subsequently proliferate and differentiate into mature neurons (3). The cardiac sympathetic nerves extend from the sympathetic neurons in stellate ganglia, which are located bilateral to the vertebra. Sympathetic nerve fibers project from the base of the heart into the myocardium and are located predominantly in the subepicardium of the ventricle. The central conduction system, which includes the sinoatrial node, atrioventricular node, and His bundle, is abundantly innervated compared with the working myocardium. We and others have reported that this regional difference in cardiac sympathetic innervation (innervation patterning) is highly conserved among mammals.

The cardiac nervous system also involves afferent nerves. The sensory signals generated in the heart are conducted through cardiac afferent nerves, primarily thinly myelinated Aδ-fibers and nonmyelinated C-fibers. The sensory nerve fibers project to the upper thoracic dorsal horn via dorsal root ganglia neurons, which are also derived from neural crest cells.

A major challenge to analysis of cardiac innervation of the heart has been the lack of suitable molecular markers. Recent advances in immunohistochemical technology now allow autonomic nerves to be stained using antibodies against nerve-specific markers, such as tyrosine hydroxylase (TH), a sympathetic marker; calcitonin gene-related peptide (CGRP), a sensory marker; protein gene product 9.5 (PGP 9.5), a general peripheral nerve marker; and growth-associated protein 43 (GAP43), a nerve sprouting marker. As discussed below, we and others have used these specific neural markers to demonstrate that the organization of cardiac innervation is strictly controlled in the heart during development, whereas in diseased hearts, innervation density and organization are dramatically altered.

Nerve sprouting and SCD

Sympathetic stimulation is important in the generation of SCD in diseased hearts. There is circadian variation in the frequency of SCD that parallels sympathetic nerve activity. β-Blocker therapy prevents SCD secondary to ventricular tachyarrhythmia in ischemic heart disease or congestive heart failure. Immunohistochemical analysis of cardiac nerves in explanted hearts of transplant recipients reveals a positive correlation between nerve density and clinical history of ventricular tachyarrhythmia (4). Zhou et al. showed that nerve growth factor (NGF), which is critical for sympathetic nerve sprouting, is upregulated after myocardial infarction (MI) in animal models, resulting in the regeneration of cardiac sympathetic nerves and heterogeneous innervation (5). In other experiments, augmented myocardial nerve sprouting through NGF infusion after MI results in a dramatic increase in SCD and a high incidence of ventricular tachyarrhythmia, compared with animals not receiving NGF infusion (6). These results demonstrate that NGF upregulation and nerve sprouting in diseased hearts may cause lethal arrhythmia and SCD. However, the molecular mechanisms that regulate NGF expression and sympathetic innervation in the heart are poorly understood.

The endothelin-1 (ET-1) / NGF pathway is critical for cardiac sympathetic innervation

In general, the growth-cone behavior of nerves is modulated by coincident signaling modulated by neural chemoattractants and chemorepellents synthesized in the innervated tissue. NGF, a potent neural chemoattractant, is a prototypic member of the neurotrophin family that plays critical roles in the differentiation, survival, and synaptic activity of the peripheral sympathetic and sensory nervous systems (7). The level of NGF expression within innervated tissue corresponds approximately to innervation density. NGF expression increases during development and is altered in diseased hearts.

ET-1 is a critical factor in the pathogenesis of cardiac hypertrophy, hypertension, and atherosclerosis. Gene targeting of ET-1 and its receptor ET_A results in un-

expected craniofacial and cardiovascular abnormalities not observed in other hypertrophic factor–deficient mice (8). Although these phenotypes are consistent with interference of neural crest differentiation, the role of ET-1 in neural crest development remains undetermined. We hypothesized that ET-1 affects the induction of neurotrophic factors and that the disruption of ET-1 contributes to the immature development of neural crest–derived cells.

We found that ET-1, but not angiotensin II, phenylephrine, leukemia inhibitory factor, or IGF-1, upregulates NGF expression in primary cultured cardiomyocytes (9). ET-1–induced NGF augmentation is not observed in cardiac fibroblasts and is specific to cardiomyocytes. ET-1–induced NGF augmentation is mediated via the ET_A receptor, $Gi\beta\gamma$, PKC, the Src family, EGFR, extracellular signal-regulated kinase, p38MAPK, activator protein-1, and the CCAAT/enhancer-binding protein δ element. To study the role of the ET-1/NGF pathway in the development of the cardiac sympathetic nervous system, we analyzed various mouse models of modified genes. NGF expression, cardiac sympathetic innervation, and norepinephrine concentration are reduced in ET-1–deficient mouse (*Edn1*$^{-/-}$) hearts, but not in the hearts of angiotensinogen-deficient mice (*Atg*$^{-/-}$). In *Edn1*$^{-/-}$ mice, the sympathetic stellate ganglia exhibited excessive apoptosis and display loss of neurons at the late embryonic stage. Moreover, we demonstrate that cardiac-specific overexpression of NGF in *Edn1*$^{-/-}$ mice rescues the heart from sympathetic nerve retardation. These findings indicate that ET-1 is a key regulator of NGF expression in cardiomyocytes and that the ET-1/NGF pathway is critical for sympathetic innervation in the heart. Given that ET-1 is strongly induced in pathological conditions, the ET-1/NGF pathway may also be involved in NGF upregulation and nerve regeneration after myocardial infarction.

NGF is critical for cardiac sensory innervation and rescues the diabetic heart from neuropathy

The cardiac autonomic nervous system is composed of efferent and afferent nerves. The cardiac sensory nervous system is responsible for pain perception and for initiating a protective cardiovascular response during myocardial ischemia. Cardiac sensory nerve impairment causes silent myocardial ischemia, which is a major cause of sudden death in DM patients. Despite the severity of this complication, the alterations in cardiac sensory innervation in diabetic sensory neuropathy and the molecular mechanism underlying this process are poorly understood. Moreover, little is known about the anatomical distribution of cardiac sensory nerves and the molecular mechanism controlling innervation during development.

Unlike somatic tissues, visceral organs, such as the heart, are believed to be rich in autonomic efferent innervation but poor in nociceptive afferent nerves. In fact, Zahner et al. report that vanilloid receptor-1–immunopositive sensory nerves are enriched in the epicardium but scarce in the myocardium (10). We show that cardiac sensory innervation is rich not only at epicardial sites but also in the ventricular myocardium and that sensory innervation increases with development (11). In a screen of several neurotrophic factors, we showed that development of cardiac sensory nerves coincides with synthesis of NGF in the heart. Cardiac nociceptive sensory nerves that are immunopositive for CGRP, including the dorsal root ganglia and the dorsal horn, are markedly retarded in NGF-deficient mice, while cardiac-specific overexpression of NGF rescues the heart from these deficits. Thus, NGF synthesis in the heart is critical for the development of the cardiac sensory nervous system.

To investigate whether NGF is involved in diabetic neuropathy, DM was induced with streptozotocin in wild-type (WT) and transgenic mice overexpressing NGF in the heart. DM-induced WT mice show downregulation of NGF, CGRP-immunopositive cardiac sensory denervation, and atrophic changes in dorsal root ganglia, whereas these defects are prevented in DM-induced NGF-transgenic mice. Cardiac sensory function, as measured by myocardial ischemia-induced c-Fos expression in dorsal root ganglia, is also downregulated by DM in WT mice, but not by DM in NGF-transgenic mice. Direct gene transfer of NGF into diabetic rat hearts improves the impaired cardiac sensory innervation and function, as determined by the electrophysiological activity of cardiac afferent nerves during myocardial ischemia. These findings demonstrate that development of the cardiac sensory nervous system depends on the synthesis of NGF in the heart, and that DM-induced suppression of NGF expression may lead to cardiac sensory neuropathy.

Phase I and phase II clinical trials showed that systemic administration of recombinant NGF is safe and has potential efficacy in diabetic polyneuropathy, but a phase III trial did not show any beneficial effects, perhaps because the dosage and route of administration were suboptimal (12, 13). The dosage of NGF was restricted by side-effects in the phase III clinical trial, and the development of anti-NGF antibodies may have contributed to the lack of beneficial effects. We examined the possibility of avoiding these complications by direct administration of the *NGF* gene to the cells that require the factor. We showed that NGF expression

and CGRP-immunopositive nerves are proportionally reduced in diabetic hearts and thus demonstrated the successful treatment of cardiac sensory neuropathy by direct *NGF* gene transfer. Consistent with our findings, the efficacy of *NGF* gene therapy has been reported in diabetic cystopathy and neuropathy of the footpad (14). Further studies on the reliability and efficacy of *NGF* gene therapy are required before clinical trials can proceed.

Sema3a is critical for cardiac sympathetic innervation patterning

As discussed above, NGF plays critical roles in cardiac nerve development. In contrast, the neural chemorepellent that induces growth-cone collapse and repels nerve axons has not been identified in the heart. The Class 3 secreted semaphorin, *Sema3a*, has been cloned and identified as a potent neural chemorepellent and a directional guidance molecule for nerve fibers (15 – 17). However, it is not known whether cardiomyocytes produce Sema3a, and if so, whether this protein affects sympathetic neural patterning and cardiac performance.

We analyzed the kinetics and distribution of cardiac sympathetic innervation in developing murine ventricles (1). TH-immunopositive sympathetic nerve endings appear on the epicardial surface at embryonic day (E)15 and gradually increase in number in the myocardium after postnatal day (P)7 and P42. In the ventricular myocardium, sympathetic nerves are more abundant in the subepicardium than in the subendocardium, suggesting an epicardial-to-endocardial gradient. We analyzed heterozygous *Sema3a* knocked-in *lacZ* mice ($Sema3a^{lacZ/+}$) to identify the *Sema3a* expression pattern and its relationship to innervation patterning in the heart. At E12, *lacZ* expression was detected strongly in the heart, especially in the trabecular components of the ventricles. In E15 hearts, *lacZ* expression was observed in the subendocardium but not in the subepicardium of the atria and ventricles (Fig. 1). At P1 and P42, *lacZ* expression was reduced in certain regions and highlighted the Purkinje fiber network along the ventricular free wall. Quantitative RT-PCR of *Sema3a* in developing

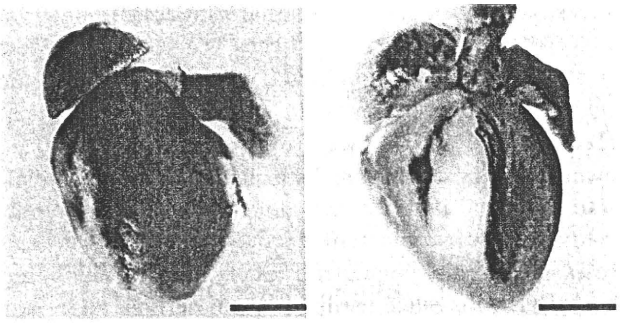

Fig. 1. *Sema3a* expression in murine hearts. X-gal staining (green) of $Sema3a^{lacZ/+}$ hearts at E15 demonstrates strong *Sema3a* expression only in the subendocardium. Scale bar = 100 μm.

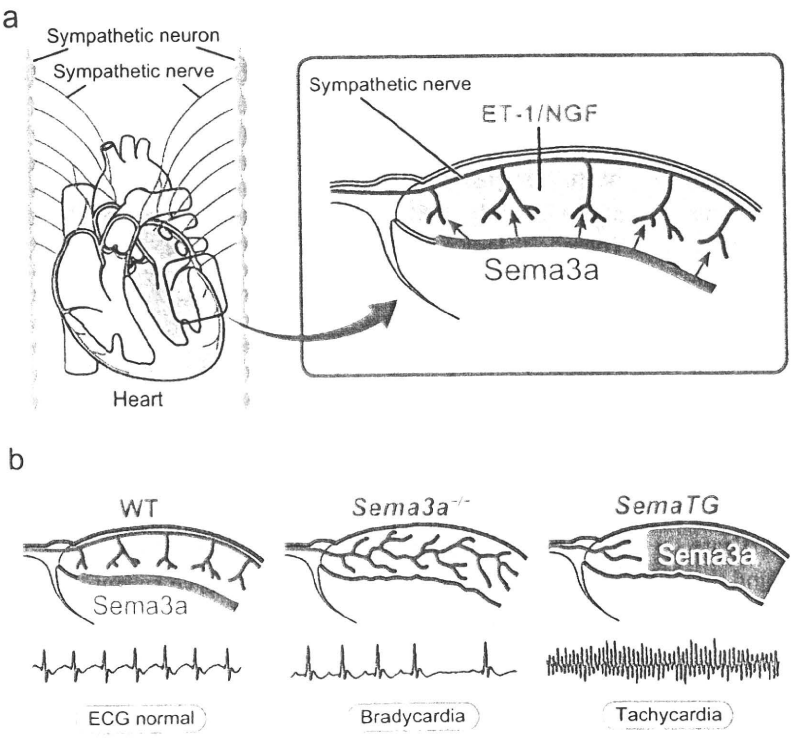

Fig. 2. Regulation of cardiac innervation patterning. a: Cardiac sympathetic innervation shows an epicardial-to-endocardial transmural gradient. This patterning is established by the balance between ET-1/NGF and Sema3a expression in the heart. Note that NGF is expressed abundantly in the working myocardium, whereas Sema3a is expressed specifically in the subendocardium. b: Appropriate Sema3a-mediated sympathetic innervation patterning is critical for the maintenance of an arrhythmia-free heart. $Sema3a^{-/-}$ mice exhibit sinus bradycardia, and *SemaTG* mice are highly susceptible to ventricular tachyarrhythmias.

hearts confirmed the presence of *Sema3a* from E12 and the subsequent linear decrease in expression. The spatial and temporal expression pattern of *Sema3a* contrasts directly with the patterning of sympathetic innervation in developing hearts. These results indicate that Sema3a is a negative regulator of cardiac innervation.

We analyzed *Sema3a*-deficient mice (*Sema3a*$^{-/-}$) to investigate whether Sema3a is critical for cardiac sympathetic nerve development. The WT hearts show a clear epicardial-to-endocardial gradient of sympathetic innervation. In contrast, the sympathetic nerve density is lower in the subepicardium and higher in the subendocardium of *Sema3a*$^{-/-}$ mice, resulting in disruption of the innervation gradient in *Sema3a*$^{-/-}$ ventricles. The *Sema3a*$^{-/-}$ mice also exhibit malformation of the stellate ganglia that extend sympathetic nerves to the heart. To investigate whether the abnormal sympathetic innervation patterning in *Sema3a*$^{-/-}$ hearts is a secondary effect of stellate ganglia malformation, we generated transgenic mice overexpressing *Sema3a* specifically in the heart (*SemaTG*). *SemaTG* mice are associated with reduced sympathetic innervation and attenuation of the epicardial-to-endocardial innervation gradient. These results indicate that cardiomyocyte-derived Sema3a plays critical roles in cardiac sympathetic innervation by inhibiting neural growth. Since cardiomyocyte-derived NGF acts as a chemoattractant, it is possible that the balance between NGF and Sema3a synthesized in the heart determines cardiac sympathetic innervation patterning.

The growth-cone behavior of somatic sensory axons is also modulated by the coincident signaling of NGF and Sema3a (18, 19). During development, NGF and Sema3a are expressed within the spinal cord and influence the guidance pathway of sensory axons. Sema3a is specifically expressed in the ventral half of the spinal cord and mediates the termination of NGF-responsive sensory axons at the dorsal part of the spinal cord. The targeted inactivation of *Sema3a* disrupts neural patterning and projections in the spinal cord, thereby highlighting the critical role of Sema3a signaling in the directional guidance of nerve fibers (17, 20).

Sema3a maintains arrhythmia-free hearts through sympathetic innervation patterning

Most *Sema3a*$^{-/-}$ mice die within the first postnatal week, with only 20% surviving until weaning. We performed telemetric electrocardiography and heart-rate variability analysis to identify the cause of death and the effects of abnormal sympathetic neural distribution in *Sema3a*$^{-/-}$ hearts (1). In addition to multiple premature ventricular contractions, *Sema3a*$^{-/-}$ mice develop sinus bradycardia and abrupt sinus arrest due to sympathetic neural dysfunction.

By comparison, the *SemaTG* mice die suddenly at 10 months of age without symptoms. Sustained ventricular tachyarrhythmia is induced in *SemaTG* mice, but not in WT mice, after epinephrine administration, and programmed electrical stimulation reveals that *SemaTG* mice are highly susceptible to ventricular tachyarrhythmia. The β_1-adrenergic receptor density is upregulated and the cAMP response after catecholamine injection is exaggerated in *SemaTG* ventricles. Action potential duration is significantly prolonged in hypoinnervated *SemaTG* ventricles, presumably via ion channel modulation. These results suggest that the higher susceptibility of *SemaTG* mice to ventricular arrhythmia is due, at least in part, to catecholamine supersensitivity and prolonged action potential duration, both of which can augment triggered activity in cardiomyocytes. Thus, Sema3a-mediated sympathetic innervation patterning is critical for the maintenance of arrhythmia-free hearts.

Sympathetic nerves modulate the function of ion channels and trigger various arrhythmias in diseased hearts (21, 22). Various studies highlight the importance of regulatory factors in sympathetic innervation patterning. For example, *Sema3a*$^{-/-}$ mice exhibit sinus bradycardia, abrupt sinus slowing, and stellate ganglia defects. Consistent with our data, right stellectomy induces sinus bradycardia and sudden, asystolic death in dogs (23). In addition, Stramba-Badiale et al. report that developmental abnormalities in cardiac innervation may play a role in the genesis of some cases of sudden infant death syndrome (24). The *SemaTG* hearts are also highly susceptible to ventricular arrhythmias, albeit without contractile dysfunction or structural defects. Given that catecholamine augments systolic function, it is surprising that *SemaTG* mice show normal cardiac function. Patients with denervated hearts who undergo heart transplantation do not develop heart failure but approximately 10% of the patients develop SCD (25). Together, these studies highlight the significance of cardiac nerve regulation as a new paradigm for the management of SCD.

Conclusions

Cardiac nerves are highly plastic, and innervation patterning is strictly controlled by the balance between NGF and Sema3a synthesized in the heart (Fig. 2a). ET-1 regulates NGF expression in cardiomyocytes, and the ET-1/NGF pathway modulates nerve sprouting and plays critical roles in sympathetic nerve development. NGF is also important in sensory nerve development, and NGF downregulation may result in sensory neuropathy in diabetic hearts. By comparison, Sema3a inhibits